Title: An altered cell-specific subcellular distribution of translesion synthesis DNA polymerase kappa (POLK) in aging neurons

Authors: Mofida Abdelmageed, Premkumar Palanisamy, Victoria Vernail, Yuval Silberman, Shilpi Paul, and Anirban Paul[#].

Corresponding author anirban@psu.edu

Affiliation: Neural and Behavioral Sciences Department, Penn State College of Medicine, Hershey, PA 17033

Abstract

Genomic stability is critical for cellular function, however, in the central nervous system highly metabolically active differentiated neurons are challenged to maintain their genome over the organismal lifespan without replication. DNA damage in neurons increases with chronological age and accelerates in neurodegenerative disorders, resulting in cellular and systemic dysregulation. Distinct DNA damage response strategies have evolved with a host of polymerases. The Y-family translesion synthesis (TLS) polymerases are well known for bypassing and repairing damaged DNA in dividing cells. However, their expression, dynamics, and role if any, in enduring postmitotic differentiated neurons of the brain are completely unknown. We show through systematic longitudinal studies for the first time that DNA polymerase kappa (POLK), a member of the Y-family polymerases, is highly expressed in neurons. With chronological age, there is a progressive and significant reduction of nuclear POLK with

a concomitant accumulation in the cytoplasm that is predictive of brain tissue age. The reduction of nuclear POLK in old brains is congruent with an increase in DNA damage markers. The nuclear POLK colocalizes with damaged sites and DNA repair proteins. The cytoplasmic POLK accumulates with stress granules and endo/lysosomal markers. Nuclear POLK expression is significantly higher in GABAergic interneurons compared to excitatory pyramidal neurons and lowest in non-neurons, possibly reflective of the inherent biological differences such as firing rates and neuronal activity. Interneurons associated with microglia have significantly higher levels of cytoplasmic POLK in old age. Finally, we show that neuronal activity itself can lead to an increase in nuclear POLK levels and a reduction of the cytoplasmic fraction. Our findings open a new avenue in understanding how different classes of postmitotic neurons deploy TLS polymerase(s) to maintain their genomic integrity over time, which will help design strategies for longevity, healthspan, and prevention of neurodegeneration.

Introduction

Throughout the organismal lifespan, continuous exposure to exogenous and endogenous agents can damage one or both strands of the DNA thus causing a persistent threat to genomic integrity (Iyama and Wilson 2013; Yan and Vaziri 2020; Chatterjee and Walker 2017; Tubbs and Nussenzweig 2017). Due to their long lifespan, increased transcriptional activity, and large energy demands, neurons are highly susceptible to cumulative DNA damage (Welch and Tsai 2022; Caldecott, Ward, and Nussenzweig 2022; Wu et al. 2021; Reid et al. 2021; Madabhushi, Pan, and Tsai 2014). Neuronal genomic enhancer regions are hotspots for constant high levels of DNA

single-strand breaks (SSBs) repair synthesis process, thus revealing that neurons are undergoing localized and continuous DNA breakage (Reid et al. 2021; Wu et al. 2021). In addition, the threat of genomic instability can also be contributed by normal “programmed” DNA breaks like topoisomerase-induced breaks for the removal of topological stress during transcription. High levels of such programmed DNA breakage occur in neurons, during development, differentiation, and maintenance (Caldecott, Ward, and Nussenzweig 2022). Recently, it was shown that programmed SSBs in the enhancer regions can be repaired by PARP1 and X-ray cross-complementing protein 1 (XRCC1)-mediated pathways (Wu et al. 2021). XRCC1 is a DNA repair scaffold protein that plays a role in multiple repair pathways including base excision repair (BER) and single-strand break repair (SSBR) (London 2020). Due to high mitochondrial activity in the neurons, which consumes about 20% of the body’s oxygen supply (Attwell and Laughlin 2001), neurons exhibit high levels of reactive oxygen species (ROS)-mediated DNA damage. ROS can damage DNA by oxidizing bases and creating abasic sites (Lindahl and Barnes 2000; Madabhushi, Pan, and Tsai 2014; Tubbs and Nussenzweig 2017). One of the most common ROS-induced DNA modifications is 8-oxo-7,8-dihydroguanine (8oxo-dG) (Amente et al. 2019; Ding, Fleming, and Burrows 2017), a lesion that is often resolved through BER (Markkanen 2017). Unrepaired SSBs hinder transcription and can also lead to DSBs. A strong association exists between unrepaired DNA damage causing loss of genomic integrity with aging and neurodegeneration (Caldecott, Ward, and Nussenzweig 2022; Welch and Tsai 2022). Hence, survival strategies have evolved to preserve genomic stability through multiple DNA damage response (DDR) pathways allowing the neurons to function effectively.

Impaired DDR leads to genomic instability triggering signaling cascades, stalling transcription, and creating mutagenesis, thus altering the cellular fate toward anomalous cell cycle activation, apoptosis, or senescence, which are hallmarks of aging and age-associated diseases (Hoeijmakers 2009; Madabhushi, Pan, and Tsai 2014; Chow and Herrup 2015; McKinnon 2017; Tubbs and Nussenzweig 2017; Welch and Tsai 2022).

One unique mechanism that bypasses DNA adducts, synthesizes DNA past damage, and functions in post-replication DNA repair is through translesion synthesis (TLS) DNA polymerases (Sale, Lehmann, and Woodgate 2012; Gao et al. 2017; Powers and Washington 2018; Lehmann 2006; Paniagua and Jacobs 2023). TLS polymerases are well-studied in dividing cells, and the Y-family TLS polymerases include Rev1, Pol kappa (Polk), Pol iota (Poli), and Pol eta (Polh) (Guo et al. 2009; Sale, Lehmann, and Woodgate 2012; Vaisman and Woodgate 2017). However, their role in postmitotic cells is not explored. There is evidence of the role of POLK in dorsal root ganglion (DRG) neurons upon the treatment of genotoxic agents like cisplatin where POLK is upregulated (Zhuo, Gorgun, and Englander 2018) and is essential for efficiently and accurately repairing cisplatin crosslinks (Jha and Ling 2018). POLK can perform error-free TLS across bulky DNA adducts at the N2 position of guanine induced by the genotoxic agent benzo[a]pyrene-dihydrodiol-epoxide (BPDE) and mitomycin C (Kanemaru et al. 2017; Ogi et al. 2002; Avkin et al. 2004). POLK can also bypass other DNA lesions including 8oxo-dG caused by oxidative stress in association with Werner syndrome helicase (WRN) protein (Haracska, Prakash, and Prakash 2002; Maddukuri et al. 2014) and through strand break repair mechanism (X. Zhang et al. 2013). *Polk*$^{-/-}$ mice showed survival defects, spontaneous mutations, and sensitivity to BPDE (Stancel

et al. 2009; Singer, Osimiri, and Friedberg 2013). Evidence supports that POLK can function in non-S phase cells through a NER-dependent mechanism to protect from UV-induced cytotoxic lesions (Ogi and Lehmann 2006; Sertic et al. 2018). *Polk*$^{-/-}$ mouse embryo fibroblasts were sensitive to hydrogen peroxide and showed defects in both SSB and DSB repair, suggesting that Polk may have an important role in the oxidative stress-induced DNA repair process (X. Zhang et al. 2013). Although POLK is associated with multiple DNA repair mechanisms, it remains unknown if normative age-associated DNA damage will also recruit POLK and how it may function in postmitotic neurons.

Unlike the long-living postmitotic neurons that endure DNA damage, the non-neuronal cells can go through the cell cycle and are replaceable. Due to the non-replicative status of differentiated neurons in mature circuits, it is critical to understand the different repair strategies and mechanisms that postmitotic neurons employ to maintain their genomic integrity, which will help design therapies for human longevity and the prevention of neurodegeneration. Here we report the expression of POLK in the brain, its subcellular localization, how it is altered with chronological age, cell type-specific variability, and the microglial engagement with neurons in wild-type mouse brains undergoing healthy aging under normative housing conditions.

Results:

A progressive age-associated shift in subcellular localization of POLK

POLK has been studied mostly in proliferating cells; however, its levels are found to be highest in the G0 phase of the cell cycle and upregulated upon exposure to exogeneous

agent cisplatin in dorsal root neurons (Zhuo, Gorgun, and Englander 2018). Hence, we explored whether POLK is expressed in the brain, where both replicating and non-replicating cells make it a unique tissue environment. Since neurons endure an onslaught of a lifetime of DNA damage due to activity, genotoxic agents, and physiological age, we investigated if the levels of endogenous POLK in the mice brain also vary as a function of age. In addition, since POLK showed subcellular relocalization in cancer cells undergoing stress (Temprine et al. 2020; Paul et al. 2022), we further explored whether POLK in the brain shows similar changes during normative aging in C57BL/6J (RRID:IMSR_JAX:000664) wild-type mice. We performed immunoblots using two independently sourced antibodies against POLK on nuclear and cytoplasmic fractions from cortical tissue of young 1 month, middle age 10 months, and early-old age 18 months mice (Figure 1A). Results showed a trend that with increasing age POLK levels decreased in the nuclear fraction, whereas there is a concomitant increase in cytoplasmic POLK (Figure 1B, S1A). However, in total cell lysate, there are no changes in POLK expression (Figure 1C, S1B). This data suggests a potential cytoplasmic relocalization of POLK with age.

To confirm the biochemical result, we used an immunofluorescence (IF) assay to visualize the spatial-temporal changes of POLK with age in a healthy wild-type mouse brain. We validated the POLK antibody, previously reported in immunofluorescence assays in human cell lines (Paul et al. 2022), using mouse primary neuronal culture and observed a significant decrease in POLK signal upon two independent siRNA knock-downs but not in scrambled siRNA (Figure S1Ci). qPCR analysis showed a 35%

reduction in *Polk* mRNA level upon siRNA knock-down (Figure S1Cii). Both antibodies showed comparable nuclear and cytoplasmic patterns and distribution of POLK in mice brains (Figure S1D). From here on onwards for all IF assays we used anti-POLK antibody SC-16667. We then conducted a longitudinal unbiased survey of POLK expression across multiple brain areas at the subcellular level using an image analysis pipeline. To visualize the changes in the subcellular level we developed an automated imaging pipeline using CellProfiler that segments the nucleus and cytoplasm using the fluorescent Nissl that primarily stains cell bodies in brain sections (C. A. Paul, Beltz, and Berger-Sweeney 2008). POLK is detected as small “speckles” inside the nucleus at a young age (1-2 months) and larger “granules” can be seen in the cytoplasm at progressively older time points (>9 months) (Figure 1D). In young brains, both the normalized counts of nuclear POLK speckles and their size are consistent across the cingulate cortex (Cg1), motor cortex (M1 and M2), and somatosensory cortex (S1). A comparison of the nuclear POLK speckle counts and size using ANCOVA shows a significant age-associated decline with medium to large effect sizes across the four brain areas surveyed (Figure 1E-G, Tables 1-2) in agreement with the immunoblot assay. On the other hand, in the cytoplasm, there is a significant age-associated accumulation of POLK in the form of increasingly larger-sized granules with decreasing total counts (Figure 1E, F, H, Tables 3-4).

To check if the age-associated decline in nuclear POLK is a more generalized phenomenon in Y-family TLS polymerases we tested the qualitative expression of REV1 and POL iota (POLI) in the mice brain. REV1 protein shows similar expression patterns as clusters of speckles inside the nucleus, a similar decline in nuclear expression, and

an increase in cytoplasmic granules in M1 and S1 brain areas at 1, 10, and 18 months (Figure 1I). Comparatively, POLI nuclear expression showed overall lower levels, with decreased age-associated alterations in nuclear expression, however still showed age-associated cytoplasmic accumulation (Figure S1E). Antibody against Pol eta (POLH) showed a very weak signal or failed. However, data from publicly available single-cell transcriptomics corroborate low transcript expression in the brain.

Nuclear POLK co-localizes with DNA damage response and repair proteins

Various pathways in the DNA damage response have evolved to detect and repair different types of lesions that threaten the genome. Among these, ROS pose a significant threat to the neurons (Attwell and Laughlin 2001), creating ROS-induced DNA modifications 8oxo-dG (Lindahl and Barnes 2000; Madabhushi, Pan, and Tsai 2014; Tubbs and Nussenzweig 2017). Repair of 8oxo-dG lesions primarily occurs through BER, where a glycosylase enzyme identifies and removes the damaged base, followed by cleavage of the DNA backbone by apurinic/apyrimidinic endonuclease 1 (APE1), resulting in a single-strand break (SSB). This intermediate can then be processed by polymerase beta (POLb) which fills in the gap with the correct nucleotide, and the nick is sealed by ligase III (LIG3). Along with single-strand breaks (SSBs), double-strand breaks (DSBs) are more harmful due to their potential for toxicity. Despite this toxicity, DSBs also play crucial roles in cellular physiology. For instance, neurons require DSBs to facilitate the expression of immediate early genes (Suberbielle et al. 2013; Madabhushi et al. 2015; Alt and Schwer 2018), particularly through transcriptional activity in postmitotic neurons. Additionally, SSBs may also lead to DSBs (Cannan and

Pederson 2016). DSB repair in postmitotic cells is predominantly managed by the non-homologous end joining (NHEJ) pathway. In canonical NHEJ, DSBs are initially recognized and bound at their ends by KU70/80 and DNA-dependent protein kinase (PRKDC). Subsequently, they are directly reconnected through ligation mediated by Ligase IV (LIG4), X-Ray Repair Cross Complementing 4 (XRCC4), and XRCC4-like factor (XLF). At DSB sites, the protein kinase ATM phosphorylates numerous downstream substrates such as histone variant H2A.X, that forms gH2AX foci, which are docking sites for DNA repair proteins like p53-binding protein 1 (53BP1) that promotes NHEJ mediated DSB repair (Mirman and Lange 2020, 5353; Panier and Boulton 2014).

There are hints that TLS polymerases including POLK play a role in NHEJ and BER in dividing cells, for example, POLK inserts the correct base opposite the 8oxo-dG lesion and extends from dC:8oxo-dG base pairs (Maddukuri et al. 2014). We previously identified DNA repair pathway proteins by performing iPoKD -MS (isolation of proteins on Pol kappa synthesized DNA followed by mass spectrometry), where proteins were captured and bound to the nascent DNA synthesized by Polk in human cell lines (Paul et al. 2022). Hence, we tested whether neuronal nuclear POLK is associated with BER and NHEJ pathway proteins identified in our iPoKD-MS data sets. We tested 5 NHEJ pathway markers and 4 BER pathway markers at middle age (9-12 months), in the wild-type mouse brain cortex and analyzed the colocalization of these proteins and the markers at the nuclear POLK sites (Figure 2A). Images from the mouse cortex with at least 3 biological replicates per age group were parsed into excitatory pyramidal

neurons (PN) and inhibitory interneurons (IN). Nissl+, NeuN+, Gad67+ cells were labeled as IN class and Nissl+, NeuN+, Gad67- as PN class neurons. Each IN and PN class cell bodies were subcellularly segmented into nucleus and cytoplasm and individual nuclear POLK speckles were identified. NHEJ and BER marker intensities were then measured within each nuclear POLK speckles (Figure 2B).

In middle age, for both IN and PN classes, we observed that POLK intensity positively correlated with DSB marker gH2AX (Figure 2C1-2), NHEJ markers 53BP1 (Figure 2D1-2) and PRKDC (Figure 2F1), and ROS-mediated damage marker 8oxo-dG (Figure 2E1-2). Interestingly, BER pathway marker APE1 and to a lesser degree LIG3 were only present in POLK speckles in INs but not in PNs (Figure 2F2-3). In the NHEJ pathway only PRKDC showed high colocalization with nuclear POLK in both IN and PN, but other NHEJ proteins like KU70 and XRCC4, did not colocalize and their intensities were not correlated with POLK levels (FigureS2).

Since both gH2AX and 8oxo-dG were positively associated with the nuclear POLK speckles we wanted to examine if their colocalization and intensity correlation with POLK levels varies with progressive age. So, we further tested early-old (18 months) and late-old (24-27 months) time points. This showed that the temporal profile of gH2AX and 8oxo-dG association with POLK are distinct. Broadly, peak colocalization of gH2AX in POLK speckles was at the early-old time point (Figure 2C3), whereas the presence of 8oxo-dG in POLK speckles declines in early-old age but strikingly increases in the late-old age group (Figure 2E3). The temporal profile of gH2AX intensities in POLK speckles

and gH2AX-POLK correlation was mirrored by 53BP1, which is well-known to promote DSB repair through NHEJ pathway, suggesting higher levels of DSBs at early-old age and spatio-temporal association of POLK. In addition, though both INs and PNs showed similar profiles, nuclear POLK speckles had consistently higher levels of gH2AX intensities in INs compared to PNs with the large effect size for 53BP1, throughout all three age groups studied (Figure 2D3), suggesting that nuclear POLK plays a role at DSB sites in INs more compared to PNs. In contrast, there was a smaller difference to ROS induced 8oxo-dG intensities between IN and PNs as well as decreased 8oxo-dG intensities in middle age (Figure 2E3). We observed POLK association with BER proteins in middle age and reduction in ROS-induced DNA damage, suggesting that POLK plays a role in BER pathway during middle age mostly in INs compared to PNs, and this capacity of POLK is lost with aging.

POLK in the cytoplasm is associated with stress granules and lysosomes in old brains

During the process of aging, protein homeostasis is known to be reduced causing widespread intracellular protein aggregates (Taylor and Dillin 2011). A decline in the protein quality control system has been shown to impact the assembly and dynamic maintenance of stress granules (SGs) leading to increased cellular aggregation. SG are nonmembrane assemblies of untranslated mRNAs, RNA-binding proteins, protein translation factors and many non-RNA-binding proteins (Cao, Jin, and Liu 2020; Guzikowski, Chen, and Zid 2019), which can be induced by oxidative stress and other stressors (Federico et al. 2012; Gandhi and Abramov 2012; Patten et al. 2010). Since

we observed that with increasing age gH2AX and 8oxo-dG are elevated (Figure 2C1-3, 2E1-3), and POLK increasingly accumulates in the cytoplasm as "granules" (Figure 1F-H), we hypothesized that cytoplasmic POLK may be present with SG. Ras-GTPase-activating protein (GAP)-binding protein 1 (G3BP1) is a key player in SG assembly often referred to as SG nucleator (Sidibé, Dubinski, and Vande Velde 2021; Aulas et al. 2015; Sahoo et al. 2018), hence we tested if cytoplasmic POLK granules colocalize with G3BP1. Further, an emerging theme in aging is that oxidative stress acts as an independent aging factor corrupting lysosome acidification leading to reduced proteolytic susceptibility of the proteins delivered to lysosomes (Nixon 2020). So, we also tested colocalization with an established endo/lysosomal marker protein lysosomal associated membrane protein 1 (LAMP1).

To characterize the nature of subcellular cytoplasmic POLK granules, we co-immunostained with SG protein G3BP1 and lysosomal protein LAMP1. In young (1-month) brains, there was a minimal expression of both G3BP1 and LAMP1, however by the early-old stage (18 months) cytoplasmic POLK is almost entirely colocalized with both G3BP1 (Figure 3A, S3A) and LAMP1 (Figure 3B, S3B) in the cytoplasm indicating that older neurons are actively accumulating non-nuclear POLK in stress granules and endo/lysosome. This suggests that with age nuclear POLK accumulates in the cytoplasmic SG and endo/lysosome.

Differentially altered POLK subcellular expression amongst excitatory, inhibitory, and non-neuronal cells in the cortex.

To further test if the subcellular shift in POLK impacts all cells uniformly, we performed immunostaining of young (1 month) and old (19-24 months) brains to segregate excitatory pyramidal neurons (PN), inhibitory interneurons (IN), and non-neuronal (NN) cells in the mouse cortex. Brain sections were co-immunostained with i) anti-NeuN to detect pan-neuronal protein RBFOX3, ii) anti-GAD67 to detect GABAergic neurons, iii) fluorescent Nissl to label all cells, and iv) anti-POLK to measure subcellular POLK levels. Our original image quantitation pipeline was modified to register cells positive for GAD67, NeuN, and Nissl as GABAergic interneurons (IN), NeuN and Nissl positives as glutamatergic excitatory pyramidal neurons (PN), and Nissl positives only as non-neuronal (NN) cells (Figure 4A). The INs and PNs were further segmented into their nuclear and cytoplasmic compartments whereas NN subcellular segmentation was not implemented due to the fact their nucleus occupies most of the cellular morphology (García-Cabezas et al. 2016) (Figure 4B). Hence in NN, the POLK signal was considered to primarily represent the nuclear compartment. We restricted our survey to the GABAergic inhibitory and glutamatergic excitatory neurons in cortical areas M1 and S1, which have no dopaminergic, serotonergic, cholinergic, glycinergic, and histaminergic neuronal cell bodies. Strikingly, at all ages across the cortical areas observed, the nuclear POLK signal was consistently highest in the cell group identified as INs, followed by PNs and NNs. ANOVA shows that these differences are highly significant with large effect sizes (Figure 4C, Table 5).

Microglia associated with IN and PN have significantly higher levels of cytoplasmic POLK

Synapses and cell bodies are removed by brain microglia and activated microglia have been associated with various neurological disorders. To test if neurons with higher cytoplasmic POLK granules are vulnerable to microglia engagement, we surveyed by immunostaining with microglia marker protein IBA1 in middle (11 months), early-old (18 months) and late-old (24-27 months) time points. Images were analyzed to register IBA1+ cells as microglia (MG class), GAD67+, NeuN+, and Nissl+ cells as IN class and NeuN+, Gad67-, and Nissl+ cells as PN class (Figure 5A). IN or PNs where MG cells are overlapping or in contact are scored as MG-tied IN or MG-tied PN, and IN and PN cell bodies that are removed by more than one MG cell body length are scored MG-free IN and MG-free PN (Figure 5B). Overall as expected, MGs are more prevalent at older ages (Figure 5C). We then compared the cytoplasmic POLK levels between the MG-tied IN and MG-free INs as well as MG-tied and MG-free PNs. Interestingly, middle and early-old MG-tied INs have significantly more cytoplasmic POLK compared to MG-free INs and MG-free PNs (Figure 5D) and higher cytoplasmic POLK granule counts in the early-old age (Figure S4). However, this effect is lost in late-old age (Figure 5D), likely due to the MG-mediated removal of the INs. Such differences were not noted in nuclear POLK counts between MG-tied and MG-free INs and PNs. Combined with the observations of elevated DNA damage and repair in INs, and higher cytoplasmic POLK levels in MG-tied INs, suggesting increased vulnerability of IN class during aging.

Subcellular localization of POLK is regulated by neuronal activity

Neuronal activity is essential for proper neuronal maturation and circuit plasticity (Yap and Greenberg 2018). High metabolic demands during increased neuronal activity can generate oxidative damage to actively transcribed regions of the genome (Lu et al. 2004). Neuronal activity-induced transcription has been linked with the generation of repeated DSBs at gene regulatory elements, potentially contributing to genome instability (Welch and Tsai 2022; Suberbielle et al. 2013; Madabhushi et al. 2015; Delint-Ramirez et al. 2022; Crowe et al. 2006). Although the coupling of transcription to DNA breaks occurs in all cell types, this process is especially challenging to long-lived neurons that are postmitotic and cannot use replication-dependent DNA repair pathways. With limited regenerative capacity, neurons are unable to replace the damaged cells (Iyama and Wilson 2013). Recently, a neuronal-specific complex NPAS4–NuA4 was identified to be bound to recurrently damaged regulatory elements and recruits additional DNA repair machinery to stimulate the repair, thus coupling neuronal activity to DNA repair (Pollina et al. 2023).

Since we observed a decrease in nuclear POLK and concomitant increase in cytoplasmic POLK with age, as well as nuclear POLK to be associated with BER and NHEJ DNA repair pathways in the mice brain, we tested if POLK subcellular localization can be regulated by neuronal activity and if this regulation is influenced by age. For this, we tested two age groups, young (1 month) where POLK was mostly localized in the nucleus as "speckles" and early-old (18 month) brains where POLK was present as large cytoplasmic "granules" and significantly lower number of nuclear speckles. Following slice electrophysiology protocol, mouse brains were extracted, and fresh

tissue was sectioned coronally and immersed in oxygenated artificial cerebrospinal fluid (ACSF) and maintained at physiological temperature. Coronal sections from the same brain were split into two groups. The control group was maintained in ASCF, and the treatment group was exposed to a bath application of kainic acid (KA), a glutamate receptor agonist that synchronously depolarizes neurons, dissolved in ACSF. Sections were exposed for a duration of 80 mins and 160 mins, tissue was fixed to terminate the experiment followed by measuring c-FOS and POLK protein levels in cells by IF (Figure 6A). c-FOS protein is known to be translated at 90 mins sustaining for 2-5 hours upon neuronal activity (Hudson 2018; Kovács 1998), and we observed a robust increase in c-FOS intensity in the nucleus at 160 mins in both young and early-old age groups (Figure 6B). Interestingly, we observed a significant increase in nuclear POLK speckle counts (Figure 6C) and a concomitant decrease in cytoplasmic POLK granules (Figure 6D) in young mice brain. However, such changes in POLK levels were not observed in early-old brains (Figure 6C-D). Since, we did not distinguish between IN, PN, and NN classes, we cannot exclude the possibility of even higher differences in activity-induced POLK subcellular localization amongst different cell classes. Thus, this data provides the first evidence of a member of the TLS family to be regulated by neuronal activity likely to retain POLK in the nucleus for activity-induced DNA repair process, a capacity that is lost with aging.

POLK as an endogenous “aging clock” for brain tissue

There have been multiple approaches towards estimating biological age using “aging clocks” using sequencing, from tissue and body fluids using epigenetic marks

(Grodstein et al. 2020) and multi-omics approach (Nie et al. 2022). Further genomic instability is increasingly associated with neuronal activity and aging, with Progeroid syndromes are often linked to genomic instability (Gurkar and Niedernhofer 2015). However, there is a lack of *in situ* methods to determine age from tissues. Hence, we hypothesized that it may be possible to use protein expression of POLK to determine the biological age of brain tissue sections. We tested if the subcellular localization of POLK can be a learnable feature that can predict organismal age from brain sections. For this, we used two related ensemble based classifiers Random Forest and Gradient Boosting Machine. Where 80% of the data was used for training and validation, and then tested on 20% hold-out group. We used data from Figure 1 and used parameters like nuclear and cytoplasmic POLK counts, nuclear area, cytoplasmic area, and replicates to examine if organismal age is discernible and found that it is indeed possible to predict 1 month, 10 months, and 18 months age brains with ROC values >0.8 (Figure 7A1 and A2). Cytoplasmic and nuclear POLK counts were the top features that drove node purity in Random Forest or Relative Influence in Boosting classifier. In addition, using data and parameters from Figure 5, where we observed the association of MG with increased cytoplasmic POLK in IN-class, we tested if finer distinctions between middle, early-old and late-old age groups are possible. Both Random Forest and Boosting classifiers were again able to distinguish between these three age groups with AUROC > 0.8, with cytoplasmic POLK median intensity and cytoplasmic granules counts per unit area as the top influencing factors (Figure 7A3 and A4).

Using a similar strategy, using data from young and old groups shown in Figure 4, we observed that in both age groups nuclear POLK speckle counts per unit area alone is

the major driver in distinguishing IN, PN, and NN classes with ROC > 0.8 (Figure 7B1 and B2), suggesting cell classes IN, PN, and NN have an inherent biological relationship in how they utilize TLS polymerase POLK.

Discussion

TLS polymerases are well-studied as DNA lesion bypass proteins in dividing cells, and recent extensive research identifies their novel roles in a myriad of other cellular processes (Anand et al. 2023; Paniagua and Jacobs 2023). Despite evidence of mRNA expression of the Y-family TLS polymerase *Polk* in IN and PN sub-types (Tasic et al. 2018; Paul et al. 2017), the role of POLK in postmitotic cells has not yet been explored in the central nervous system (CNS). There is only one study of POLK in the peripheral nervous system (PNS), where upon cisplatin treatment *Polk* mRNA was upregulated in dorsal root ganglion (DRG) neurons (Zhuo, Gorgun, and Englander 2018), and POLK was found essential for efficiently and accurately repairing cisplatin crosslinks (Jha and Ling 2018). In a cell-free system, POLK faithfully bypasses 8oxo-dG (Maddukuri et al. 2014), which is a major DNA lesion in the neurons. Interestingly, *Polk*$^{-/-}$ mice showed decreased survival compared to wild-type (WT) and heterozygous littermates, and increased levels of spontaneous mutations (Stancel et al. 2009). Separately, inactivated *Polk* knock-in mice showed a higher frequency of mutations, micronucleated cells, and DNA damage marker gH2AX foci compared to WT *Polk* mice (Takeiri et al. 2014). In these studies, effect of *Polk*$^{-/-}$ was not explored in the brain. However, *apoE−/−;Polk−/−* mice showed enhanced DNA mutagenesis in several organs including the brain probably due to cholesterol-induced adducts (Singer, Osimiri, and Friedberg 2013).

Evidence supports that POLK can function in non-S phase cells through a NER-dependent mechanism to protect from UV-induced cytotoxic lesions (Ogi and Lehmann 2006; Sertic et al. 2018). Given that DNA damage markers 8oxo-dG and gH2AX are highly correlated with aging, and Polk is associated with multiple DNA repair mechanisms, it remains unknown if normative age-associated DNA damage will also recruit POLK and how it may function in post-mitotic neurons. This is the first systematic and longitudinal study of Y-family TLS polymerase focusing mostly on the POLK in neurons.

Here, we found that Y-family TLS polymerases including POLK are highly expressed in several cortical brain areas with characteristic nuclear speckle-like distribution, reminiscent of nuclear foci in dividing cells (Bi et al. 2005; Bergoglio et al. 2002, 1). Surprisingly, we noted that even in the absence of any exogenous chemical or behavioral stressors, in wild-type mice, POLK in neurons localizes to the cytoplasm at least as early as 10-11 months (middle age) and continues to do so with further normative aging. In fact, this nuclear to cytoplasm POLK relocalization signal is so robust and reproducible that we could train two ensemble learning models to predict age of the mice brain, where cytoplasmic and nuclear POLK counts were the primary featured drivers. Both learning models performed comparatively well, with possible applications as *in situ* immunofluorescence-based physiological “aging clocks”. This can be complementary to existing sequencing-based epigenetic clocks (de Lima Camillo, Lapierre, and Singh 2022; Bell et al. 2019; Prosz et al. 2024; Griffin et al. 2024; Varshavsky et al. 2023; Kerepesi et al. 2021), allowing simultaneous visual read-out of

brain tissue age while scoring for various markers for neurodegeneration, cell stress, and age-associated neuropathologies. We believe other TLS proteins may behave similarly and a combinatorial approach can even increase the age-predictive power. We were able to make even finer distinctions among middle, early, and late-old stages using the cytoplasmic POLK intensity signal.

Our findings showing progressive loss of nuclear POLK and accumulation in the cytoplasm suggest nuclear POLK plays an important role in protecting neurons from DNA damage at a young age. Decline of nuclear POLK is likely correlated with lack of repair leading to DNA damage accumulation during the normative aging process. Our data further confirms nuclear POLK is associated with neuronal DNA damage as observed by colocalization with DSB (gH2AX) and ROS-mediated DNA damage sites (8oxo-dG), as well as POLK's role in the BER (colocalization with APE1 and LIG3) and NHEJ repair pathways (53BP1 and PRKDC) in the neurons. Association with PRKDC further suggests POLK's role in the "gap-filling" step in the NHEJ repair pathway in neurons.

Compared to replicating cells, the functional role of DNA damage in non-replicating neuronal senescence remains elusive. In addition, an enduring question revolves around the differential vulnerability of neuronal subtypes to DNA damage (Welch and Tsai 2022). Remarkably, we observed POLK's nuclear expression to be cell class-specific, with the highest in INs followed by PN and NN. INs and PNs engage in highly demanding cellular functions, both transcriptionally and energetically. While other

important and more abundant cell types in the nervous system, such as astrocytes, oligodendrocytes, and microglia, collectively grouped in this study as NN are also vulnerable to DNA damage, but their characteristics differ significantly from neurons. For instance, NNs can be dispensed as they are largely renewable, possess relatively lower energy demands due to slower physiological kinetics, and can re-enter the cell cycle when necessary (Welch and Tsai 2022). These attributes are thought to collectively lessen the dependence of DNA damage repair in glial cells compared to neurons. Hence the observed lowest nuclear expression of POLK in NN at face value can be reconciled with their known biology. On the other hand, a significant fraction of the IN-types like PV basket cells, Chandelier cells, and Martinotti cells across cortical areas have fast-firing kinetics and hence are energetically more demanding (Markram et al. 2004; Tremblay, Lee, and Rudy 2016) arguably accumulating more damage and DNA adducts may require highest nuclear POLK presence. Here too, the disparity of nuclear POLK was reproducible enough across young and older ages that measuring the nuclear POLK speckle counts per unit area can predict cell class identity using ensemble learning with a consistently high AUROC values exceeding 0.8.

The association between neurons harboring DNA damage, age-associated neuroinflammation and cell-type vulnerability is an important piece of the puzzle to understand age-associated neurodegeneration under normal physiological conditions (Welch and Tsai 2022). We observed progressive accumulation of cytoplasmic POLK in stress granules and endo/lysosomal compartments with age. Interestingly, microglia-associated INs, MG-tied INs, have significantly higher cytoplasmic POLK suggesting

they are more vulnerable to cumulative age-associated changes. One possibility is that the decline in nuclear POLK in INs causes a reduction in DNA repair that may further initiate cGAS-STING immune signaling thereby recruiting microglia (Gulen et al. 2023; Talbot et al. 2023) or higher levels of cytoplasmic POLK may itself lead to immune activation. Further in-depth molecular mechanistic studies are needed to dissect POLK's role in neuronal cell class-specific genome maintenance and how it intersects with microgliosis during aging.

Another factor contributing to the heightened vulnerability of neurons to genomic damage is their involvement in functional processes like neuronal activity. Such as induced activity of primary neurons with bicuculline or exposure of mice to fear learning was shown to generate DSBs at the promoters of immediate-early genes (Madabhushi et al. 2015; Stott, Kritsky, and Tsai 2021) and even mice experiencing a new environment can induce DSBs in neurons (Suberbielle et al. 2013). These activity-induced DSBs are thought to aid in the expression of immediate early genes by swiftly resolving topological constraints at their transcription start sites. Here, we showed inducing neuronal activity in slice culture increases nuclear POLK while diminishing cytoplasmic accumulation. This shows for the first time that POLK is responsive to neuronal activity, and we speculate an increase in nuclear POLK is likely to be involved in activity-induced DSBs. However, we noticed that this effect is lost during the process of aging. Thus, in our study, we provide first-time evidence of Y-family TLS polymerase, POLK's differential expression in CNS cell classes, and its age-associated and activity-

induced subcellular changes with implications in microgliosis under non-pathogenic aging conditions.

Figure legends:

Figure 1: POLK subcellular expression changes with increasing age, across multiple cortical regions.

A) Experimental design to longitudinally compare POLK cellular localization in mice brains.

B) Western blot of nuclear and cytoplasmic fractions from mice cortex in three age groups (each with three biological replicates). Nuclear POLK was detected normalized with histone levels and cytoplasmic POLK normalized to GAPDH. In nuclear fraction, a

band above between 75-100 kDa and in cytoplasmic fraction bands between 75-200 kDa are seen.

C) Western blot of whole cell lysates from mouse brain cortex for each age time points using three biological replicates. A single POLK band was detected between 75-100 kDa and was normalized to tubulin.

D) Immunofluorescence (IF) followed by imaging and analysis using Cell Profiler of mouse brain sections. Visualization of POLK speckles (green) expression using immunohistochemistry in cells labeled by fluorescent-nissl (red) from wild-type mouse brain aged 1 month, and 18 months. Subcellular compartments were segmented and POLK was detected and measured separately inside the nucleus and in the cytoplasm.

E) Representative low (20x) and high magnification (63x) images of Polk expression using IF from Cg1, M1, M2, and S1 cortical regions in ages 1 month (N=3), 10 months (N=2), and 18 months (N=3). POLK (green) and Nissl depicting all cells (purple) (scale bar = 10um).

F) Boxplot showing nuclear and cytoplasmic POLK counts per unit area for each brain region in 1C grouped by age. n denotes the numbers of cells measured per time points under each boxplot.

G) Means plots with 95% confidence intervals showing the nuclear POLK speckle count and size decreasing with increasing age in Cg1, M1, M2, and S1 cortical areas.

H) Means plots with 95% confidence intervals show the cytoplasmic POLK granule count decreasing with a concomitant increase in size with age in Cg1, M1, M2, and S1 cortical areas.

I) Representative low (20x) and high magnification (63x) images of REV1 expression using IF from S1 and M1 cortical regions in ages 1 month, 10 months, and 18 months. REV1 (green) and Nissl depicting all cells (purple) (scale bar = 10um in 20x image). Arrowheads point nuclear speckles and arrows indicate cytoplasmic granules.

Figure 2. Colocalization and coexpression of POLK with DNA damage marker proteins in POLK nuclear speckles

A) Experimental design to longitudinally compare POLK colocalization with various DNA damage markers in three age group mice brains. Asterix denotes markers that were studied in three age groups, rest were evaluated in middle age only.

B) Schematic of cell class gating logic, registration, sub-cellular segmentation, POLK speckle detection, measurement of POLK counts, and POLK and DNA damage markers/repair protein intensities.

C1) Representative images showing colocalization of gH2AX, and channel separation of POLK, gH2AX, and POLK speckle overlay on POLK and gH2AX. POLK speckles detected inside the nucleus are outlined in yellow. IN class cells are outlined in red, PN class in green.

C2) Scatterplots of gH2AX intensity measured inside POLK nuclear speckle (y-axis) were plotted against POLK intensities (x-axis) shown for INs (red) and PNs (green). The correlation coefficient and p-values are indicated for each.

C3) Dot mean plots with 95% confidence error bars of gH2AX intensities in the y-axis in INs (red) and PNs (green) plotted as a function of age (x-axis).

D1) Representative images showing colocalization of 53BP1, and channel separation of POLK, 53BP1, and POLK speckle overlay on POLK and 53BP1. POLK speckles detected inside the nucleus are outlined in yellow. IN class cells are outlined in red, and PN class in green.

D2) Scatterplots of 53BP1 intensity measured inside POLK nuclear speckle (y-axis) were plotted against POLK intensities (x-axis) shown for INs (red) and PNs (green). The correlation coefficient and p-values are indicated for each.

D3) Dot mean plots with 95% confidence error bars of 53BP1 intensities in the y-axis in INs (red) and PNs (green) plotted as a function of age (x-axis).

E1) Representative images showing colocalization of 8oxo-dG, and channel separation of POLK, 8oxo-dG, and POLK speckle overlay on POLK and 8oxo-dG. POLK speckles detected inside the nucleus are outlined in yellow. IN class cells are outlined in red, and PN class in green.

E2) Scatterplots of 8oxo-dG intensity measured inside POLK nuclear speckle (y-axis) were plotted against POLK intensities (x-axis) shown for INs (red) and PNs (green). The correlation coefficients and p-values are indicated for each.

E3) Dot mean plots with 95% confidence error bars of 8oxo-dG intensities in the y-axis in INs (red) and PNs (green) plotted as a function of age (x-axis).

F1-F3) Left column, merged 63X representative images of IN and PN, with red arrowheads showing line scan area where intensities of POLK and PRKDC (F1), POLK and APE1 (F2), and POLK and LIG3 (F3) were measured. The right columns in F1-F3 shows corresponding IN and PN-derived scatterplots where y-axis shows PRKDC

intensities (F1), APE1 (F2), LIG3 (F3), plotted against POLK intensities (x-axis). Separate plots shown for INs (red) and PNs (green). The correlation coefficients and p-values are indicated for each.

Figure 3: Cytoplasmic POLK expression co-localizing with stress granules and lysosomal proteins

A) Cytoplasmic POLK (green) expression co-localizing with G3BP1 (blue) in fluorescent-nissl stained cells (purple) of mouse brain tissue from M1 and S1 cortical regions in 18 months old brain but not in young 1 month.

B) Cytoplasmic POLK (green) expression co-localizing with LAMP1 (blue) in fluorescent-nissl stained cells (purple) of mouse brain tissue from M1 and S1 cortical regions of 18-month brain.

Figure 4: Nuclear POLK is differentially expressed based on cell-type in old brains.

A) Representative image of the detection of inhibitory interneurons (IN), excitatory pyramidal neurons (PN) and non-neuronal (NN) cell bodies using automated image analysis pipeline from a four-channel image of cortical areas.

B) Magnified view of the dotted box from subpanel A showing overlay of the nuclear, cytoplasmic segmentation outlines and detection of nuclear POLK speckles and cytoplasmic POLK granules in IN, PN, and NN cells from wild-type mice cortical areas M1 and S1.

C) Boxplots from brain areas show the nuclear POLK count is higher in INs than PNs and NNs across cortical areas in both young and old age groups.

Figure 5: Microglia associated with INs and PNs show significantly higher levels of cytoplasmic POLK expression.

A) Schematic of the experimental design showing age groups, cell class gating logic, scoring spatial interaction, subcellular segmentation, detection, and measurement of POLK in the cytoplasmic compartment.

B) A representative single 20x imaging field shows outlines of detected cell bodies of IN (red), PN (green). Iba1+ microglia (MG) that are attached or wrapped to neurons (MG-tied, filled light pink and arrows) and microglia that are within one body length of a neuron (blue fill with an asterisk) as well as unassociated microglia (blue fill). Channel separation shown for the four-channel super-resolution confocal image, fluorescent-nissl, NeuN, and Gad67 = IN, fluorescent-nissl, and NeuN = PN, and fluorescent-nissl, and Iba1 = MG.

C) Representative images from M1 and S1 cortical areas shows an overall increase in Iba1-positive cells in early old age compared to young. Yellow arrowheads point to MG-tied neurons.

D) Boxplot showing the difference in cytoplasmic POLK granule median intensity between MG-free and MG-tied INs and PNs across middle, early old, and late old time age groups. T-test p-values and effect sizes are shown for each comparison.

Figure 6: Kainic acid-induced neuronal activity causes POLK subcellular localization in young ex-vivo brain.

A) Schematic of the experimental design showing age groups, ex-vivo treatment of kainic acid, and control groups, followed by, immunostaining, imaging, and the measurement of nuclear and cytoplasmic POLK.

B) Boxplot of cFOS levels between ACSF control and kainic acid-treated groups at 80min and 160min post-exposure intervals between young and old brains. t-Test shows a robust and significant cFOS level increase at 160min in both age groups.

C) Boxplot of nuclear POLK speckle counts per unit between ACSF control and kainic acid-treated groups at 80min and 160min post-exposure intervals between young and old brains. t-Test shows a significant increase in nuclear POLK at 160min in the young brains.

D) Boxplot of cytoplasmic POLK granule counts per unit area between ACSF control and kainic acid-treated groups at 80min and 160min post-exposure intervals between young and old brains. T-test shows there is a significant decrease in cytoplasmic granule counts upon kainic acid treatment after 160min in young brains.

E) Boxplot of cytoplasmic POLK granule size measured by area contained, between ACSF control and kainic acid-treated groups at 80min and 160min post-exposure intervals between young and old brains. T-test shows there is a significant but tiny decrease in cytoplasmic granule counts upon kainic acid treatment after 160min in young brains.

Figure 7: Subcellular expression of POLK is a learnable feature predictive of organismal age and IN, PN, and NN cell class from mouse brain tissue.

A1-2) Random Forest (A1) and Gradient Boosting (A2) classifier can distinguish between 1-month, 10-month, and 18-month-old age groups upon training on the subcellular nuclear and cytoplasmic distribution of POLK counts using data from figure 1F and 1G. Top bar shows the number of cells used for training, validation, and test samples of the total. Area Under Receiver Operator Curve (AUROC) values show the performance of the classifier for each age group when tested on the holdout groups. The bar plot shows the relative contribution of the image parameters and image metadata indicating cytoplasmic POLK counts as the major driver.

A3-4) Random Forest (A3) and Gradient Boosting (A4) classifier can distinguish between middle to late-old ages 10-month, 18-month, and 24-27-month age groups upon training on the subcellular nuclear and cytoplasmic distribution of POLK counts, POLK intensities in nuclear speckles and cytoplasmic granules, MG association and other metadata from figure 5. Top bar shows the data split for training, validation and test groups. Major driver of performance is cytoplasmic POLK intensity and counts.

B1-2) Random Forest (B1) and Gradient Boosting (B2) classifier can distinguish between broad IN, PN, and NN cell class with high AUROC values. Nuclear POLK per unit area and nuclear area are the major feature drivers of performance.

Acknowledgments: Work was supported by grant NIH RF1AG072602 / R01AG072602 to AP and Startup Funds from Penn State College of Medicine to A.P.

Author contributions: AP conceived, directed, and planned the work. AP and SP designed the experiments. MA, PP, AP, and SP performed experiments. VV and YS helped MA and PP with experiments with slice preparation and kainic acid experiments. MA, PP, AP, and SP did the analysis, and generated figures. AP wrote the manuscript with help from SP. All authors discussed the results and commented on the manuscript.

Supplemental Figure Legends

Figure S1 associated with Figure 1

S1A(i) Western blot of nuclear and cytoplasmic fractions from mouse brain cortex in 3months, 10months, and 18-month-aged brains of all three biological replicates using Abclonal antibody (A12052), a portion of which is displayed in main Figure 1B.

S1A(ii) Western blot of nuclear and cytoplasmic fractions from mouse brain cortex in 3months, 10months, and 18-month mouse cortex using Santa Cruz antibody (SC-16667).

S1B) Total cell lysates of all three biological replicates from 3-month, 10-month, and 18 months mouse cortex, a portion of which is displayed in main Figure 1C.

S1C(i) Immunofluorescence staining with anti-POLK antibody with SC-16667 on mouse primary neuronal cultures treated with Polk siRNA (top row) showing a marked reduction in nuclear POLK levels after 48hrs, compared to scrambled siRNA control (bottom row).

S1C(ii) qPCR of Polk transcript shows a 35% reduction upon siRNA against Polk but not scrambled control siRNA. Polh mRNA levels were not affected by siRNA against Polk.

S1D) Immunofluorescence staining of wild-type 18-month-old mouse, from brain cortical area S1 shows a similar pattern and distribution of POLK nuclear speckles (arrowheads) and cytoplasmic granules (arrows). The bottom row is a crop of the boxed area in the corresponding top image.

S1E) Immunofluorescence staining of wild-type mouse brain cortical areas S1 and M1 also shows POLI punctate nuclear expression resembling speckles and progressive cytoplasmic accumulation with age at 10 and 18 months.

Supplement Figure S2 associated with Figure 2: Scatter plots showing intensity-intensity plots from INs (red) and PNs (green), where y-axis is KU70, XRCC1, and XRCC4, intensity levels plotted against POLK intensities in the x-axis. The correlation coefficients and p-values are indicated for each.

Supplement Figure S3 associated with Figure 3: Additional representative image with channel separation for immunofluorescence staining of wild-type mouse brain cortical areas S1, showing cytoplasmic POLK is colocalized with stress granule marker G3BP1 and endo/lysosomal marker LAMP1. Arrows indicate few representative sites of colocalization in both images.

Supplement Figure S4 associated with Figure 5: Boxplots comparing the nuclear POLK median intensity and cytoplasmic POLK granule count between MG-free and MG-tied INs and PNs across middle, early-old, and late-old time age groups. T-test p-values are shown for each comparison.

Methods

List of antibodies

Reagent	Designation	Source	Identifier	Dilution
Antibody	Mouse anti-PolK	Santa Cruz	Cat #: sc-16667	IF (1:200 & 1:400) WB (1:500)
Antibody	Mouse anti-PolK	Abclonal	Cat#A12052	IF (1:8000) WB (1:2000)
Antibody	Mouse anti-REV1	Santa Cruz	Cat #: sc-393022	IF (1:400)
Antibody	Mouse anti-PolI	Santa Cruz	Cat #: sc-101026	IF (1:400)
Antibody	Guinea Pig anti-NeuN/Fox3	Synaptic Systems	Cat #: 266004	IF (1:500)
Antibody	Mouse anti-Gad67	Millipore	Cat#: MAB5406	IF (1:1000)
Antibody	Rabbit anti-Gamma h2ax	Novus Biologicals	Cat#: NB100-384	IF (1:2000)
Antibody	Rabbit anti-53BP1	Novus Biologicals	Cat #: NB100-304	IF (1:2000)
Antibody	Rabbit anti-8-OHdG	GeneTex	Cat #: GTX35250	IF (1:100)
Antibody	Rabbit anti-DNA-PKcs	ABclonal	Cat #: A7716	IF (1:100)
Antibody	Rabbit anti-XRCC4	ABclonal	Cat #: A18046	IF (1:100)
Antibody	Rabbit anti-DNA Ligase III	ABclonal	Cat #: A13507	IF (1:100)
Antibody	Rabbit anti-Ku70	ABclonal	Cat #: A7330	IF (1:100)
Antibody	Rabbit anti-XRCC1	ABclonal	Cat #: A0442	IF (1:100)
Antibody	Rabbit anti-Ape1	ABclonal	Cat #: A11238	IF (1:100)
Antibody	Rabbit anti-Iba1	abcam	Cat #: AB178846	IF (1:1000)
Antibody	Mouse anti-G3BP1	DSHB	Cat #: PCRP-G3BP1-2H8	IF (1:18)
Antibody	Rat anti-1D4B	DSHB	Cat #: AB_528127	IF (1:200)
Antibody	Rabbit anti-cFOS	Synaptic Systems	Cat #: 226008	IF (1:1000)
Antibody	Dylight 405 Goat anti-Guinea Pig	Jackson ImmunoResearch	Cat #: 106475003	IF (1:1000)
Antibody	Alex Fluor 488 Goat anti-	Invitrogen	Cat #: A21121	IF (1:1000 & 1:2000)

	Mouse IgG1			
Antibody	Alex Fluor 488 Donkey anti-Mouse IgG	Invitrogen	Cat #: A32814	IF (1:1000)
Antibody	Alex Fluor 594 Goat anti-Mouse IgG2a	Invitrogen	Cat #: A21135	IF (1:1000)
Antibody	Alex Fluor 594 Goat anti-Rat	Invitrogen	Cat #: A48264	IF (1:1000)
Antibody	Alex Fluor 647 Goat anti-Rabbit	Invitrogen	Cat #: A32733	IF (1:1000)
NeuroTrace 435/455 blue-fluorescent Nissl stain	Nucleic Acids	Invitrogen	Cat #: N21479	IF (1:300)
NeuroTrace 640/660 deep red-fluorescent Nissl stain	Nucleic Acids	Invitrogen	Cat #:N21483	IF (1:300)
Antibody	Alpha Tubulin	Proteintech	Cat #: HRP-66031	WB (1:10,000)
Antibody	GAPDH	Santa Cruz	Cat #: sc-365062	WB (1:2000)
Antibody	Histone-H3	Santa Cruz	Cat #: sc-517576	WB (1:1000)

Animals

Animal use approved and overseen by Penn State College of Medicine Institutional Animal Care and Committee and the Penn State College of Medicine Comparative Medicine. The following mouse lines were used: wild-type C57/BL6 (Jackson Laboratory, Stock#000664) and *Gad2*$^{tm2(cre)Zjh}$/J (Jackson Laboratory, Stock#010802). Mice were housed in a temperature and humidity-controlled environment in a barrier facility. Mice were kept under a standard 12 h light–dark cycle, with food and water provided ad libitum. For experiments, animals were used at 1-3 months, 9-12 months, 18-19 months, and 24–27 months of age.

Primary Neuronal Culture

Mouse cortical neuronal cultures (Thermo Scientific, Cat No. A15585) were obtained from Thermo Scientific and prepared according to the manufacturer's methods with minor modifications. Briefly, the frozen cells were rapidly thawed and resuspended in complete Neurobasal™ Medium (Cat No. 21103049, Gibco™) containing B-27™ Supplement (Cat No. 17504044, Gibco™) and GlutaMAX™ Supplement (Cat No. 35050061, Gibco™). The cells were counted, and then cell suspensions were seeded at 50,000–250,000 cells/cm² on CC2 Glass 0.7 cm² 8-well chamber slides (Nunc™ Lab-Tek™ II CC2™ Chamber Slide System, Thermo Scientific, Cat No. 154941). The chamber slides were kept in a 5% CO2 incubator at 37°C. After 24 hours, half of the media from each well was aspirated and replaced with fresh media. The cells were fed every third day by aspirating half of the medium from each well and replacing it with fresh medium.

siRNA Transfection and Immunocytochemistry

At DIV10, transfection of primary neuronal culture with siRNA was performed using manufacturer's protocol (Horizon Dharmacon). Briefly, 1 uM of Accell siRNA was mixed with Accell siRNA delivery media and added to the neurons containing complete Neurobasal media (50/50 v/v). siRNA used : Accell Mouse Polk siRNA (Cat No. A-048146-13-0050, Dharmacon) or Accell Red Non-targeting siRNA (Cat No. D-001960-01-05, Dharmacon), or Accell Non-targeting siRNA pool (Cat No. D-001910-10-05, Dharmacon). A second method of transfection was used using Lipofectamine RNAiMAX reagent (Thermofisher), OptiMEM (Gibco) following manufacturer's protocol. siRNA used: DinB siRNA (m) (sc-60538) and Control siRNA-A (Cat No. sc-37007). Cells were incubated with the siRNA complex in Opti-MEM for 6 hours, followed by replacement with complete Neurobasal media.
At 24, 48, and 72 hours after transfection, cortical primary neuronal cells were washed with DPBS+ (DPBS with Ca^{2+} and Mg^{2+}) and fixed with 4% paraformaldehyde for 20 minutes at room temperature. They were then washed with DPBS+ three times. The permeabilization step was achieved using 0.3% Triton™ X-100 (diluted in DPBS+) for 5 minutes at room temperature, followed by incubation in blocking solution (DPBS+ containing 5% goat serum and 0.3% Triton™ X-100) for 1 hour. Cells were washed and incubated with respective primary antibodies (Table-1) overnight. The next day, the cells were incubated with appropriate secondary antibodies (Table-2) for 1 hour. The slides were washed, and the chambers were separated from the glass slide. Cells were stained with DAPI and Hoechst Nucleic Acid Stains (Cat No. H3570, ThermoFisher Scientific), covered with a coverslip using a mounting medium, and stored at 4°C. Images were taken using a confocal microscope (LSM) and analyzed using NIH ImageJ software. Experiments were repeated a minimum of three times, with details provided under figure legends.

Immunofluorescence Assay

Mice were anesthetized with 100-200ul of ketamine and underwent transcardiac perfusion using 1x phosphate buffered saline (PBS, 10x diluted to 1x from Corning, Cat No. 46-013-CM) and 4% paraformaldehyde (PFA, Electron Microscopy Sciences, Cat No. 19208) made in 0.2M PBS. Brain tissue were fixed with 4% PFA at 4°C degrees for 24hours, post-fixation brains were transferred to 1% sodium azide (Scientific inc., Cat No. DSS24080-250) in 1xPBS. Fixed brains were sectioned coronally at 60µm thickness using a vibratome. For staining, free-floating brain slices underwent blocking consisting of 10% goat serum (Jackson ImmunoResearch, Cat No. 005000121), 1x PBS, and 10% Triton X-100 (Thermo Scientific, Cat No. A16046) at RT for 2 hours on an orbital shaker. Following blocking slices were washed 3x with PBS at RT for 10 minutes each time. Slices were incubated with cocktail mix of 1xPBS, 1% Triton X, 5% goat serum, and primary antibody 4°C degrees for 24hours on an orbital shaker. Post-primary incubation, slices were wash 3x with PBS at RT for 10 minutes each time. Slices were incubated with 1xPBS, 1% Triton X, 5% goat serum, and secondary antibody at RT for 2 hours on an orbital shaker. Slices were washed for 10 minutes on orbital shaker at RT. Slices were incubated with 1xPBS and Nissl for 40 minutes at RT, followed by a final wash with 1xPBS for 10 minutes. Slices were mounted on ColorFrost Microscope slides using mounting media (Invitrogen, Cat No. E142757). Immunofluorescence assay in figure 1 used a slightly different procedure. The blocking buffer using 10% donkey serum instead of goat serum.

Protein extraction and Western blot analysis

Total protein extracts from the mouse brain cortex were prepared using the N-PER™ Neuronal Protein Extraction Reagent (Thermo Scientific, Cat No. 87792) following the manufacturer's instructions. Nuclear and cytoplasmic proteins from brain cortex tissues were extracted using the Minute™ Cytosolic and Nuclear Extraction Kit for Frozen/Fresh Tissues (Invent Biotechnologies INC, Cat No. NT-032), also following the manufacturer's instructions. Protein

concentration was determined using the Pierce™ BCA Protein Assay Kit (Thermo Scientific, Cat No. 23227). Protein samples were boiled at 95 °C with 4x Laemmli sample buffer (Bio-Rad, Cat No. 1610747) for 5 minutes. Samples were separated on 4–20% Mini-PROTEAN® TGX™ Precast Protein Gels (Bio-Rad) and transferred to a 0.45 µm LF PVDF membrane using the Trans-Blot® Turbo™ Transfer System (Bio-Rad, Cat No. 1704274). After blocking with 5% non-fat dry milk in phosphate-buffered saline with 0.1% Tween 20 for 1 hour at room temperature, membranes were incubated overnight at 4 °C with primary antibodies: Polk (ABclonal), Polk-HRP (Santa Cruz Biotechnology), Alpha Tubulin, GAPDH, and Histone-H3. Blots were further incubated with secondary antibody (HRP-conjugated anti-mouse IgG, 1:10,000) for 1 hour. Bands were detected using SuperSignal™ West Pico PLUS Chemiluminescent Substrate (Thermo Scientific) and scanned using the ChemiDoc Imaging System (Bio-Rad). Quantitative analyses were performed using Image J software (NIH). Proteins were normalized to the corresponding loading control.

Confocal Microscopy, Image Analysis, Quantification

Imaging was performed using Zeiss LSM910 with AiryScan2 super-resolution in multiplex mode SR-2Y, using 40X water (NA=1.2) and 63X oil (NA=1.4) objectives. All images were captured at 16-bit depth. For the 40X objective, scaling per pixel is 0.078um x 0.078um with an image size of 4084 x 4084 pixels. The scaling for the 63X objective is 0.035um x 0.035um per pixel with an image size of 2860 x 2860 pixels. The imaging parameters such as laser power, digital gain, digital offset, and scan-speed were kept constant for all samples within each experiment. Images were saved as uncompressed .czi files, and imported into the CellProfiler v4.2.6 software, where cells were registered, subcellularly segmented and POLK nuclear speckles and cytoplasmic granules were detected as individual objects and quantified.

Statistical Analysis

Statistical analysis, t-test, ANVOA, ANCOVA, Random Forest and Boosting Classifier were done using opensource software JASP 0.18.3, R Studio v2023.06.1+524, and GraphPad Prism. Plots were generated using R Studio, JASP, and GraphPad exported and composed in Adobe Illustrator.

***Ex Vivo* kainic acid treatment**

Brains from 1-month and 18-month-old C57BL/6J animals were dissected and immediately placed on ice. Brains were placed on the mount and cut through the midline, separating each hemisphere. 1.5% agar was prepared and used for the mold of the brain. The brains were submerged in the ice-cold, oxygenated sucrose dissecting solution (in mM: 183 sucrose, 20 NaCl, 0.5 KCl, 1 MgCl2, 1.4 NaH2PO4, 25 NaHCO3, and 10 glucose). Coronal hemi-slices of 100µm-thickness for IF experiments were prepared using a Compresstome® VF-310-0Z (Precisionary Instruments, LLC) with a double-edged stainless-steel blade. Both hemi-slices were placed in an oxygenated holding solution with a modified artificial cerebrospinal fluid (ACSF) (in mM: 100 sucrose, 60 NaCl, 2.5 KCl, 1.4 NaH2PO4, 1.1 CaCl2, 3.2 MgCl2, 1.2 MgSO4, 22 NaHCO3, 20 glucose, 1 ascorbic acid) for 14 minutes. After 14 minutes, the hemi-slices for control were transferred to an oxygenated standard ACSF solution (in mM: 124 NaCl, 4.4 KCl, 2CaCl2, 2.95 MgSO4, 1 NaH2PO4, 10 glucose, 26 NaHCO3) at 28–32°C. The treatment group received bath application of 1.0uM kainic acid (KA, Millipore Sigma, Cat No. K0250) dissolved in ACSF. Control and KA treated slices were removed from the bath at 80 minutes, and 160 minutes. For IF experiments, slices were fixed in 4% PFA for 30 minutes followed by storage in 1% sodium azide to proceed with IF protocol.

Figure generation: All representative images from the Zeiss .czi files were exported as TIFFs or JPEGs using FIJI, and CellProfiler. Graphical plots were exported as PDFs from RStudio, JASP, or GraphPad Prism, and subpane

Bibliography

Alt, Frederick W., and Bjoern Schwer. 2018. “DNA Double-Strand Breaks as Drivers of Neural Genomic Change, Function, and Disease.” *DNA Repair* 71 (November):158–63. https://doi.org/10.1016/j.dnarep.2018.08.019.

Amente, Stefano, Giacomo Di Palo, Giovanni Scala, Tiziana Castrignanò, Francesca Gorini, Sergio Cocozza, Angela Moresano, et al. 2019. “Genome-Wide Mapping of 8-Oxo-7,8-Dihydro-2’-Deoxyguanosine Reveals Accumulation of Oxidatively-Generated Damage at DNA Replication Origins within Transcribed Long Genes of Mammalian Cells.” *Nucleic Acids Research* 47 (1): 221–36. https://doi.org/10.1093/nar/gky1152.

Anand, Jay, Lilly Chiou, Carly Sciandra, Xingyuan Zhang, Jiyong Hong, Di Wu, Pei Zhou, and Cyrus Vaziri. 2023. “Roles of Trans-Lesion Synthesis (TLS) DNA Polymerases in Tumorigenesis and Cancer Therapy.” *NAR Cancer* 5 (1): zcad005. https://doi.org/10.1093/narcan/zcad005.

Attwell, D., and S. B. Laughlin. 2001. “An Energy Budget for Signaling in the Grey Matter of the Brain.” *Journal of Cerebral Blood Flow and Metabolism: Official Journal of the International Society of Cerebral Blood Flow and Metabolism* 21 (10): 1133–45. https://doi.org/10.1097/00004647-200110000-00001.

Aulas, Anaïs, Guillaume Caron, Christos G. Gkogkas, Nguyen-Vi Mohamed, Laurie Destroismaisons, Nahum Sonenberg, Nicole Leclerc, J. Alex Parker, and Christine Vande Velde. 2015. “G3BP1 Promotes Stress-Induced RNA Granule Interactions to Preserve Polyadenylated mRNA.” *Journal of Cell Biology* 209 (1): 73–84. https://doi.org/10.1083/jcb.201408092.

Avkin, Sharon, Moshe Goldsmith, Susana Velasco-Miguel, Nicholas Geacintov, Errol C. Friedberg, and Zvi Livneh. 2004. “Quantitative Analysis of Translesion DNA Synthesis across a Benzo[a]Pyrene-Guanine Adduct in Mammalian Cells: THE ROLE OF DNA POLYMERASE κ *.” *Journal of Biological Chemistry* 279 (51): 53298–305. https://doi.org/10.1074/jbc.M409155200.

Bell, Christopher G., Robert Lowe, Peter D. Adams, Andrea A. Baccarelli, Stephan Beck, Jordana T. Bell, Brock C. Christensen, et al. 2019. “DNA Methylation Aging Clocks: Challenges and Recommendations.” *Genome Biology* 20 (1): 249. https://doi.org/10.1186/s13059-019-1824-y.

Bergoglio, Valérie, Clarisse Bavoux, Vincent Verbiest, Jean-Sebastien Hoffmann, and Christophe Cazaux. 2002. “Localisation of Human DNA Polymerase Kappa to Replication Foci.” *Journal of Cell Science* 115 (Pt 23): 4413–18. https://doi.org/10.1242/jcs.00162.

Bi, Xiaohui, Damien M. Slater, Haruo Ohmori, and Cyrus Vaziri. 2005. “DNA Polymerase Kappa Is Specifically Required for Recovery from the Benzo[a]Pyrene-Dihydrodiol Epoxide (BPDE)-Induced S-Phase Checkpoint.” *The Journal of Biological Chemistry* 280 (23): 22343–55. https://doi.org/10.1074/jbc.M501562200.

Caldecott, Keith W., Michael E. Ward, and André Nussenzweig. 2022. “The Threat of Programmed DNA Damage to Neuronal Genome Integrity and Plasticity.” *Nature Genetics* 54 (2): 115–20. https://doi.org/10.1038/s41588-021-01001-y.

Cannan, Wendy J., and David S. Pederson. 2016. “Mechanisms and Consequences of Double-Strand DNA Break Formation in Chromatin.” *Journal of Cellular Physiology* 231 (1): 3–14. https://doi.org/10.1002/jcp.25048.

Cao, Xiuling, Xuejiao Jin, and Beidong Liu. 2020. “The Involvement of Stress Granules in Aging and Aging□associated Diseases.” *Aging Cell* 19 (4): e13136. https://doi.org/10.1111/acel.13136.

Chatterjee, Nimrat, and Graham C. Walker. 2017. “Mechanisms of DNA Damage, Repair, and Mutagenesis.” *Environmental and Molecular Mutagenesis* 58 (5): 235–63. https://doi.org/10.1002/em.22087.

Chow, Hei-man, and Karl Herrup. 2015. “Genomic Integrity and the Ageing Brain.” *Nature Reviews. Neuroscience* 16 (11): 672–84. https://doi.org/10.1038/nrn4020.

Crowe, Samantha L., Vilen A. Movsesyan, Timothy J. Jorgensen, and Alexei Kondratyev. 2006. “Rapid Phosphorylation of Histone H2A.X Following Ionotropic Glutamate Receptor Activation.” *The European Journal of Neuroscience* 23 (9): 2351–61. https://doi.org/10.1111/j.1460-9568.2006.04768.x.

Delint-Ramirez, Ilse, Lahiri Konada, Lance Heady, Richard Rueda, Alvaro Sebastian Vaca Jacome, Eric Marlin, Charlotte Marchioni, et al. 2022. “Calcineurin Dephosphorylates Topoisomerase IIβ and Regulates the Formation of Neuronal-Activity-Induced DNA Breaks.” *Molecular Cell* 82 (20): 3794-3809.e8. https://doi.org/10.1016/j.molcel.2022.09.012.

Ding, Yun, Aaron M. Fleming, and Cynthia J. Burrows. 2017. “Sequencing the Mouse Genome for the Oxidatively Modified Base 8-Oxo-7,8-Dihydroguanine by OG-Seq.” *Journal of the American Chemical Society* 139 (7): 2569–72. https://doi.org/10.1021/jacs.6b12604.

Federico, Antonio, Elena Cardaioli, Paola Da Pozzo, Patrizia Formichi, Gian Nicola Gallus, and Elena Radi. 2012. “Mitochondria, Oxidative Stress and Neurodegeneration.” *Journal of the Neurological Sciences* 322 (1–2): 254–62. https://doi.org/10.1016/j.jns.2012.05.030.

Gandhi, Sonia, and Andrey Y. Abramov. 2012. “Mechanism of Oxidative Stress in Neurodegeneration.” *Oxidative Medicine and Cellular Longevity* 2012:428010. https://doi.org/10.1155/2012/428010.

Gao, Yanzhe, Elizabeth Mutter-Rottmayer, Anastasia Zlatanou, Cyrus Vaziri, and Yang Yang. 2017. “Mechanisms of Post-Replication DNA Repair.” *Genes* 8 (2): 64. https://doi.org/10.3390/genes8020064.

García-Cabezas, Miguel Á., Yohan J. John, Helen Barbas, and Basilis Zikopoulos. 2016. “Distinction of Neurons, Glia and Endothelial Cells in the Cerebral Cortex: An Algorithm Based on Cytological Features.” *Frontiers in Neuroanatomy* 10. https://www.frontiersin.org/articles/10.3389/fnana.2016.00107.

Griffin, Patrick T., Alice E. Kane, Alexandre Trapp, Jien Li, Matthew Arnold, Jesse R. Poganik, Ryan J. Conway, et al. 2024. “TIME-Seq Reduces Time and Cost of DNA Methylation Measurement for Epigenetic Clock Construction.” *Nature Aging* 4 (2): 261–74. https://doi.org/10.1038/s43587-023-00555-2.

Grodstein, Francine, Bernardo Lemos, Lei Yu, Artemis Iatrou, Philip L. De Jager, and David A. Bennett. 2020. “Characteristics of Epigenetic Clocks Across Blood and Brain Tissue in Older Women and Men.” *Frontiers in Neuroscience* 14:555307. https://doi.org/10.3389/fnins.2020.555307.

Gulen, Muhammet F., Natasha Samson, Alexander Keller, Marius Schwabenland, Chong Liu, Selene Glück, Vivek V. Thacker, et al. 2023. “cGAS–STING Drives Ageing-Related Inflammation and Neurodegeneration.” *Nature* 620 (7973): 374–80. https://doi.org/10.1038/s41586-023-06373-1.

Guo, Caixia, J. Nicole Kosarek-Stancel, Tie-Shan Tang, and Errol C. Friedberg. 2009. “Y-Family DNA Polymerases in Mammalian Cells.” *Cellular and Molecular Life Sciences: CMLS* 66 (14): 2363–81. https://doi.org/10.1007/s00018-009-0024-4.

Gurkar, Aditi U., and Laura J. Niedernhofer. 2015. “Comparison of Mice with Accelerated Aging Caused by Distinct Mechanisms.” *Experimental Gerontology*, Proceedings of the Twelfth International Symposium on the Neurobiology and Neuroendocrinology of Aging, Bregenz, Austria July 27–August 1, 2014, 68 (August):43–50. https://doi.org/10.1016/j.exger.2015.01.045.

Guzikowski, Anna R., Yang S. Chen, and Brian M. Zid. 2019. “Stress-Induced mRNP Granules: Form and Function of Processing Bodies and Stress Granules.” *Wiley Interdisciplinary Reviews. RNA* 10 (3): e1524. https://doi.org/10.1002/wrna.1524.

Haracska, Lajos, Louise Prakash, and Satya Prakash. 2002. “Role of Human DNA Polymerase Kappa as an Extender in Translesion Synthesis.” *Proceedings of the National Academy of Sciences of the United States of America* 99 (25): 16000–5. https://doi.org/10.1073/pnas.252524999.

Hoeijmakers, Jan H. J. 2009. “DNA Damage, Aging, and Cancer.” *The New England Journal of Medicine* 361 (15): 1475–85. https://doi.org/10.1056/NEJMra0804615.

Hudson, Andrew E. 2018. “Genetic Reporters of Neuronal Activity: C-Fos and G-CaMP6.” *Methods in Enzymology* 603:197–220. https://doi.org/10.1016/bs.mie.2018.01.023.

Iyama, Teruaki, and David M. Wilson. 2013. “DNA Repair Mechanisms in Dividing and Non-Dividing Cells.” *DNA Repair* 12 (8): 620–36. https://doi.org/10.1016/j.dnarep.2013.04.015.

Jałoszyński, Paweł, Eiji Ohashi, Haruo Ohmori, and Susumu Nishimura. 2005. “Error-Prone and Inefficient Replication across 8-Hydroxyguanine (8-Oxoguanine) in Human and Mouse Ras Gene Fragments by DNA Polymerase Kappa.” *Genes to Cells: Devoted to Molecular & Cellular Mechanisms* 10 (6): 543–50. https://doi.org/10.1111/j.1365-2443.2005.00858.x.

Jha, Vikash, and Hong Ling. 2018. “Structural Basis for Human DNA Polymerase Kappa to Bypass Cisplatin Intrastrand Cross-Link (Pt-GG) Lesion as an Efficient and Accurate Extender.” *Journal of Molecular Biology* 430 (11): 1577–89. https://doi.org/10.1016/j.jmb.2018.04.023.

Kamiya, Hiroyuki, and Masahiro Kurokawa. 2012. “Mutagenic Bypass of 8-Oxo-7,8-Dihydroguanine (8-Hydroxyguanine) by DNA Polymerase κ in Human Cells.” *Chemical Research in Toxicology* 25 (8): 1771–76. https://doi.org/10.1021/tx300259x.

Kanemaru, Yuki, Tetsuya Suzuki, Akira Sassa, Kyomu Matsumoto, Noritaka Adachi, Masamitsu Honma, Satoshi Numazawa, and Takehiko Nohmi. 2017. “DNA Polymerase Kappa Protects Human Cells against MMC-Induced Genotoxicity through Error-Free Translesion DNA Synthesis.” *Genes and Environment* 39 (January):6. https://doi.org/10.1186/s41021-016-0067-3.

Kerepesi, Csaba, Bohan Zhang, Sang-Goo Lee, Alexandre Trapp, and Vadim N. Gladyshev. 2021. “Epigenetic Clocks Reveal a Rejuvenation Event during Embryogenesis Followed by Aging.” *Science Advances* 7 (26): eabg6082. https://doi.org/10.1126/sciadv.abg6082.

Kovács, K. J. 1998. “C-Fos as a Transcription Factor: A Stressful (Re)View from a Functional Map.” *Neurochemistry International* 33 (4): 287–97. https://doi.org/10.1016/s0197-0186(98)00023-0.

Lehmann, Alan R. 2006. “Translesion Synthesis in Mammalian Cells.” *Experimental Cell Research* 312 (14): 2673–76. https://doi.org/10.1016/j.yexcr.2006.06.010.

Lima Camillo, Lucas Paulo de, Louis R. Lapierre, and Ritambhara Singh. 2022. “A Pan-Tissue DNA-Methylation Epigenetic Clock Based on Deep Learning.” *Npj Aging* 8 (1): 1–15. https://doi.org/10.1038/s41514-022-00085-y.

Lindahl, T., and D. E. Barnes. 2000. “Repair of Endogenous DNA Damage.” *Cold Spring Harbor Symposia on Quantitative Biology* 65:127–33. https://doi.org/10.1101/sqb.2000.65.127.

London, Robert E. 2020. “XRCC1 - Strategies for Coordinating and Assembling a Versatile DNA Damage Response.” *DNA Repair* 93 (September):102917. https://doi.org/10.1016/j.dnarep.2020.102917.

Lu, Tao, Ying Pan, Shyan-Yuan Kao, Cheng Li, Isaac Kohane, Jennifer Chan, and Bruce A. Yankner. 2004. “Gene Regulation and DNA Damage in the Ageing Human Brain.” *Nature* 429 (6994): 883–91. https://doi.org/10.1038/nature02661.

Madabhushi, Ram, Fan Gao, Andreas R. Pfenning, Ling Pan, Satoko Yamakawa, Jinsoo Seo, Richard Rueda, et al. 2015. “Activity-Induced DNA Breaks Govern the Expression of Neuronal Early-Response Genes.” *Cell* 161 (7): 1592–1605. https://doi.org/10.1016/j.cell.2015.05.032.

Madabhushi, Ram, Ling Pan, and Li-Huei Tsai. 2014. “DNA Damage and Its Links to Neurodegeneration.” *Neuron* 83 (2): 266–82. https://doi.org/10.1016/j.neuron.2014.06.034.

Maddukuri, Leena, Amit Ketkar, Sarah Eddy, Maroof K. Zafar, and Robert L. Eoff. 2014. “The Werner Syndrome Protein Limits the Error-Prone 8-Oxo-dG Lesion Bypass Activity of Human DNA Polymerase Kappa.” *Nucleic Acids Research* 42 (19): 12027–40. https://doi.org/10.1093/nar/gku913.

Markkanen, Enni. 2017. “Not Breathing Is Not an Option: How to Deal with Oxidative DNA Damage.” *DNA Repair* 59 (November):82–105. https://doi.org/10.1016/j.dnarep.2017.09.007.

Markram, Henry, Maria Toledo-Rodriguez, Yun Wang, Anirudh Gupta, Gilad Silberberg, and Caizhi Wu. 2004. “Interneurons of the Neocortical Inhibitory System.” *Nature Reviews. Neuroscience* 5 (10): 793–807. https://doi.org/10.1038/nrn1519.

McKinnon, Peter J. 2017. “Genome Integrity and Disease Prevention in the Nervous System.” *Genes & Development* 31 (12): 1180–94. https://doi.org/10.1101/gad.301325.117.

Mirman, Zachary, and Titia de Lange. 2020. “53BP1: A DSB Escort.” *Genes & Development* 34 (1–2): 7–23. https://doi.org/10.1101/gad.333237.119.

Nie, Chao, Yan Li, Rui Li, Yizhen Yan, Detao Zhang, Tao Li, Zhiming Li, et al. 2022. “Distinct Biological Ages of Organs and Systems Identified from a Multi-Omics

Study." *Cell Reports* 38 (10): 110459. https://doi.org/10.1016/j.celrep.2022.110459.
Nixon, Ralph A. 2020. "The Aging Lysosome: An Essential Catalyst for Late-Onset Neurodegenerative Diseases." *Biochimica Et Biophysica Acta. Proteins and Proteomics* 1868 (9): 140443. https://doi.org/10.1016/j.bbapap.2020.140443.
Ogi, Tomoo, and Alan R. Lehmann. 2006. "The Y-Family DNA Polymerase Kappa (Pol Kappa) Functions in Mammalian Nucleotide-Excision Repair." *Nature Cell Biology* 8 (6): 640–42. https://doi.org/10.1038/ncb1417.
Ogi, Tomoo, Yoichi Shinkai, Kiyoji Tanaka, and Haruo Ohmori. 2002. "Polkappa Protects Mammalian Cells against the Lethal and Mutagenic Effects of Benzo[a]Pyrene." *Proceedings of the National Academy of Sciences of the United States of America* 99 (24): 15548–53. https://doi.org/10.1073/pnas.222377899.
Paniagua, Inés, and Jacqueline J. L. Jacobs. 2023. "Freedom to Err: The Expanding Cellular Functions of Translesion DNA Polymerases." *Molecular Cell* 83 (20): 3608–21. https://doi.org/10.1016/j.molcel.2023.07.008.
Panier, Stephanie, and Simon J. Boulton. 2014. "Double-Strand Break Repair: 53BP1 Comes into Focus." *Nature Reviews Molecular Cell Biology* 15 (1): 7–18. https://doi.org/10.1038/nrm3719.
Patten, David A., Marc Germain, Melissa A. Kelly, and Ruth S. Slack. 2010. "Reactive Oxygen Species: Stuck in the Middle of Neurodegeneration." *Journal of Alzheimer's Disease: JAD* 20 Suppl 2:S357-367. https://doi.org/10.3233/JAD-2010-100498.
Paul, Anirban, Megan Crow, Ricardo Raudales, Miao He, Jesse Gillis, and Z. Josh Huang. 2017. "Transcriptional Architecture of Synaptic Communication Delineates GABAergic Neuron Identity." *Cell* 171 (3): 522-539.e20. https://doi.org/10.1016/j.cell.2017.08.032.
Paul, Carol Ann, Barbara Beltz, and Joanne Berger-Sweeney. 2008. "The Nissl Stain: A Stain for Cell Bodies in Brain Sections." *Cold Spring Harbor Protocols* 2008 (9): pdb.prot4805. https://doi.org/10.1101/pdb.prot4805.
Pollina, Elizabeth A., Daniel T. Gilliam, Andrew T. Landau, Cindy Lin, Naomi Pajarillo, Christopher P. Davis, David A. Harmin, et al. 2023. "A NPAS4–NuA4 Complex Couples Synaptic Activity to DNA Repair." *Nature* 614 (7949): 732–41. https://doi.org/10.1038/s41586-023-05711-7.
Powers, Kyle T., and M. Todd Washington. 2018. "Eukaryotic Translesion Synthesis: Choosing the Right Tool for the Job." *DNA Repair* 71 (November):127–34. https://doi.org/10.1016/j.dnarep.2018.08.016.
Prosz, Aurel, Orsolya Pipek, Judit Börcsök, Gergely Palla, Zoltan Szallasi, Sandor Spisak, and István Csabai. 2024. "Biologically Informed Deep Learning for Explainable Epigenetic Clocks." *Scientific Reports* 14 (1): 1306. https://doi.org/10.1038/s41598-023-50495-5.
Reid, Dylan A., Patrick J. Reed, Johannes C. M. Schlachetzki, Ioana I. Nitulescu, Grace Chou, Enoch C. Tsui, Jeffrey R. Jones, et al. 2021. "Incorporation of a Nucleoside Analog Maps Genome Repair Sites in Postmitotic Human Neurons." *Science (New York, N.Y.)* 372 (6537): 91–94. https://doi.org/10.1126/science.abb9032.
Sahoo, Pabitra K., Seung Joon Lee, Poonam B. Jaiswal, Stefanie Alber, Amar N. Kar, Sharmina Miller-Randolph, Elizabeth E. Taylor, et al. 2018. "Axonal G3BP1

Stress Granule Protein Limits Axonal mRNA Translation and Nerve Regeneration." *Nature Communications* 9 (1): 3358. https://doi.org/10.1038/s41467-018-05647-x.

Sale, Julian E., Alan R. Lehmann, and Roger Woodgate. 2012. "Y-Family DNA Polymerases and Their Role in Tolerance of Cellular DNA Damage." *Nature Reviews Molecular Cell Biology* 13 (3): 141–52. https://doi.org/10.1038/nrm3289.

Sertic, Sarah, Antonio Mollica, Ilaria Campus, Stefania Roma, Emanuela Tumini, Andrés Aguilera, and Marco Muzi-Falconi. 2018. "Coordinated Activity of Y Family TLS Polymerases and EXO1 Protects Non-S Phase Cells from UV-Induced Cytotoxic Lesions." *Molecular Cell* 70 (1): 34-47.e4. https://doi.org/10.1016/j.molcel.2018.02.017.

Shilpi Paul, Abbey Rebok, Paolo Cifani, Anirban Paul, Darryl Pappin, Tony T. Huang, and Thomas E. Spratt. 2022. "Translesion DNA Synthesis Polymerase κ Is Essential to a Carcinogen-Induced Nucleolar Stress Response." *bioRxiv*, January, 2022.10.27.513845. https://doi.org/10.1101/2022.10.27.513845.

Sidibé, Hadjara, Alicia Dubinski, and Christine Vande Velde. 2021. "The Multi-Functional RNA-Binding Protein G3BP1 and Its Potential Implication in Neurodegenerative Disease." *Journal of Neurochemistry* 157 (4): 944–62. https://doi.org/10.1111/jnc.15280.

Singer, William D., Lindsey C. Osimiri, and Errol C. Friedberg. 2013. "Increased Dietary Cholesterol Promotes Enhanced Mutagenesis in DNA Polymerase Kappa-Deficient Mice." *DNA Repair* 12 (10): 817–23. https://doi.org/10.1016/j.dnarep.2013.07.010.

Stancel, J. Nicole Kosarek, Lisa D. McDaniel, Susana Velasco, James Richardson, Caixia Guo, and Errol C. Friedberg. 2009. "Polk Mutant Mice Have a Spontaneous Mutator Phenotype." *DNA Repair* 8 (12): 1355–62. https://doi.org/10.1016/j.dnarep.2009.09.003.

Stott, Ryan T., Oleg Kritsky, and Li-Huei Tsai. 2021. "Profiling DNA Break Sites and Transcriptional Changes in Response to Contextual Fear Learning." *PLOS ONE* 16 (7): e0249691. https://doi.org/10.1371/journal.pone.0249691.

Suberbielle, Elsa, Pascal E. Sanchez, Alexxai V. Kravitz, Xin Wang, Kaitlyn Ho, Kirsten Eilertson, Nino Devidze, Anatol C. Kreitzer, and Lennart Mucke. 2013. "Physiologic Brain Activity Causes DNA Double-Strand Breaks in Neurons, with Exacerbation by Amyloid-β." *Nature Neuroscience* 16 (5): 613–21. https://doi.org/10.1038/nn.3356.

Takeiri, Akira, Naoko A. Wada, Shigeki Motoyama, Kaori Matsuzaki, Hiromi Tateishi, Kaoru Matsumoto, Naoko Niimi, et al. 2014. "In Vivo Evidence That DNA Polymerase Kappa Is Responsible for Error-Free Bypass across DNA Cross-Links Induced by Mitomycin C." *DNA Repair* 24 (December):113–21. https://doi.org/10.1016/j.dnarep.2014.09.002.

Talbot, Emily J, Lisha Joshi, Peter Thornton, Mahya Dezfouli, Kalliopi Tsafou, Michael Perkinton, and Svetlana V Khoronenkova. 2023. "cGAS-STING Signalling Regulates Microglial Chemotaxis in Genome Instability." *Nucleic Acids Research* 52 (3): 1188–1206. https://doi.org/10.1093/nar/gkad1184.

Tasic, Bosiljka, Zizhen Yao, Lucas T. Graybuck, Kimberly A. Smith, Thuc Nghi Nguyen, Darren Bertagnolli, Jeff Goldy, et al. 2018. "Shared and Distinct Transcriptomic

Cell Types across Neocortical Areas." *Nature* 563 (7729): 72–78. https://doi.org/10.1038/s41586-018-0654-5.
Taylor, Rebecca C., and Andrew Dillin. 2011. "Aging as an Event of Proteostasis Collapse." *Cold Spring Harbor Perspectives in Biology* 3 (5): a004440. https://doi.org/10.1101/cshperspect.a004440.
Temprine, Kelsey, Nathaniel R. Campbell, Richard Huang, Erin M. Langdon, Theresa Simon-Vermot, Krisha Mehta, Averill Clapp, Mollie Chipman, and Richard M. White. 2020. "Regulation of the Error-Prone DNA Polymerase Polκ by Oncogenic Signaling and Its Contribution to Drug Resistance." *Science Signaling* 13 (629). https://doi.org/10.1126/scisignal.aau1453.
Tremblay, Robin, Soohyun Lee, and Bernardo Rudy. 2016. "GABAergic Interneurons in the Neocortex: From Cellular Properties to Circuits." *Neuron* 91 (2): 260–92. https://doi.org/10.1016/j.neuron.2016.06.033.
Tubbs, Anthony, and André Nussenzweig. 2017. "Endogenous DNA Damage as a Source of Genomic Instability in Cancer." *Cell* 168 (4): 644–56. https://doi.org/10.1016/j.cell.2017.01.002.
Vaisman, Alexandra, and Roger Woodgate. 2017. "Translesion DNA Polymerases in Eukaryotes: What Makes Them Tick?" *Critical Reviews in Biochemistry and Molecular Biology* 52 (3): 274–303. https://doi.org/10.1080/10409238.2017.1291576.
Varshavsky, Miri, Gil Harari, Benjamin Glaser, Yuval Dor, Ruth Shemer, and Tommy Kaplan. 2023. "Accurate Age Prediction from Blood Using a Small Set of DNA Methylation Sites and a Cohort-Based Machine Learning Algorithm." *Cell Reports Methods* 3 (9): 100567. https://doi.org/10.1016/j.crmeth.2023.100567.
Welch, Gwyneth, and Li-Huei Tsai. 2022. "Mechanisms of DNA Damage-Mediated Neurotoxicity in Neurodegenerative Disease." *EMBO Reports* 23 (6): e54217. https://doi.org/10.15252/embr.202154217.
Wu, Wei, Sarah E. Hill, William J. Nathan, Jacob Paiano, Elsa Callen, Dongpeng Wang, Kenta Shinoda, et al. 2021. "Neuronal Enhancers Are Hotspots for DNA Single-Strand Break Repair." *Nature* 593 (7859): 440–44. https://doi.org/10.1038/s41586-021-03468-5.
Yan, Shan, and Cyrus Vaziri. 2020. "An Introduction for the Special Issue on Environmental Health and Genome Integrity." *Environmental and Molecular Mutagenesis* 61 (7): 660–63. https://doi.org/10.1002/em.22400.
Yap, Ee-Lynn, and Michael E. Greenberg. 2018. "Activity-Regulated Transcription: Bridging the Gap between Neural Activity and Behavior." *Neuron* 100 (2): 330–48. https://doi.org/10.1016/j.neuron.2018.10.013.
Zhang, Xiuli, Lingna Lv, Qian Chen, Fenghua Yuan, Ting Zhang, Yeran Yang, Hui Zhang, et al. 2013. "Mouse DNA Polymerase Kappa Has a Functional Role in the Repair of DNA Strand Breaks." *DNA Repair* 12 (5): 377–88. https://doi.org/10.1016/j.dnarep.2013.02.008.
Zhang, Y., F. Yuan, X. Wu, M. Wang, O. Rechkoblit, J. S. Taylor, N. E. Geacintov, and Z. Wang. 2000. "Error-Free and Error-Prone Lesion Bypass by Human DNA Polymerase Kappa in Vitro." *Nucleic Acids Research* 28 (21): 4138–46. https://doi.org/10.1093/nar/28.21.4138.

Zhuo, Ming, Murat F. Gorgun, and Ella W. Englander. 2018. “Translesion Synthesis DNA Polymerase Kappa Is Indispensable for DNA Repair Synthesis in Cisplatin Exposed Dorsal Root Ganglion Neurons.” *Molecular Neurobiology* 55 (3): 2506–15. https://doi.org/10.1007/s12035-017-0507-5.

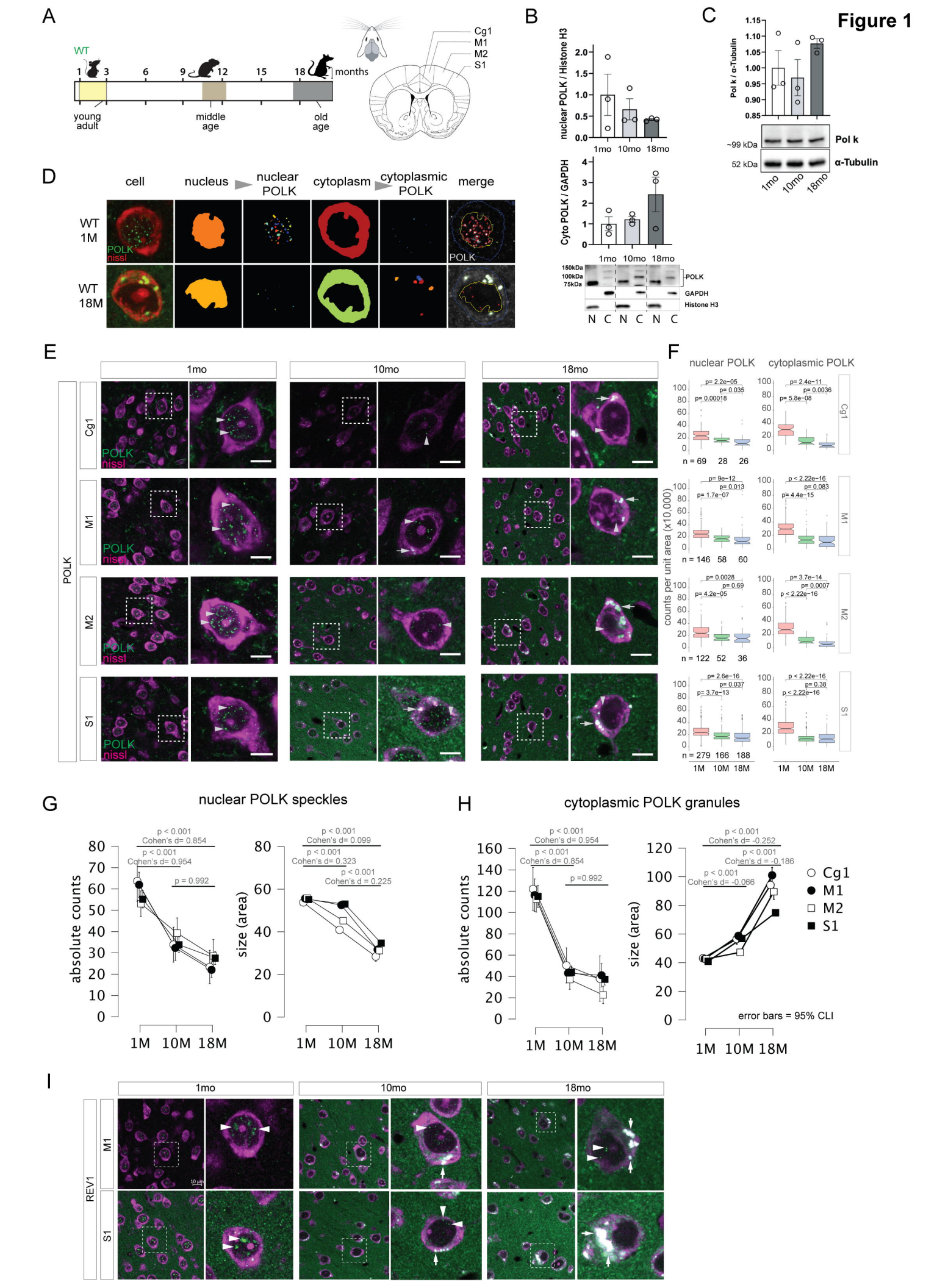
Figure 1
A
WT
1 3 6 9 12 15 18 months
young adult
middle age
old age
Cg1
M1
M2
S1
B
nuclear POLK / Histone H3
1mo 10mo 18mo
Cyto POLK / GAPDH
150kDa
100kDa
75kDa
POLK
GAPDH
Histone H3
N C N C N C
C
Pol k / α-Tubulin
~99 kDa
52 kDa
Pol k
α-Tubulin
1mo 10mo 18mo
D
cell
nucleus
nuclear POLK
cytoplasm
cytoplasmic POLK
merge
WT 1M
WT 18M
POLK
nissl
E
1mo
10mo
18mo
POLK
Cg1
M1
M2
S1
F
nuclear POLK
cytoplasmic POLK
counts per unit area (x10,000)
n = 69 28 26
n = 146 58 60
n = 122 52 36
n = 279 166 188
1M 10M 18M
G
nuclear POLK speckles
absolute counts
size (area)
p < 0.001
Cohen's d= 0.854
Cohen's d= 0.954
p = 0.992
Cohen's d= 0.099
Cohen's d= 0.323
Cohen's d = 0.225
1M 10M 18M
H
cytoplasmic POLK granules
Cohen's d= 0.954
Cohen's d= 0.854
Cohen's d= -0.252
Cohen's d = -0.186
Cohen's d= -0.066
Cg1
M1
M2
S1
error bars = 95% CLI
I
REV1
M1
S1
10 µm

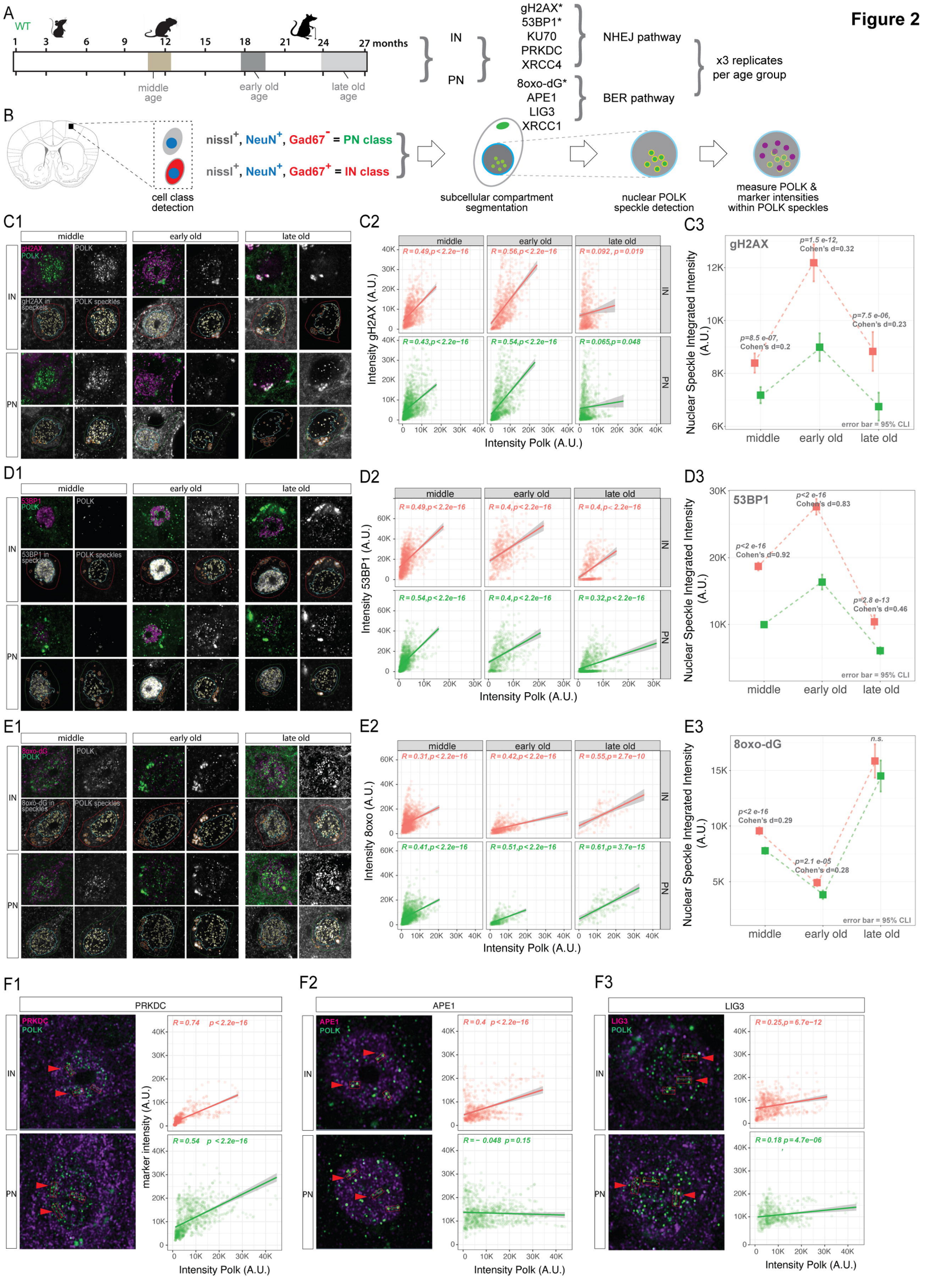
Figure 2
A
WT
1 3 6 9 12 15 18 21 24 27 months
middle age
early old age
late old age
IN
PN
gH2AX*
53BP1*
KU70
PRKDC
XRCC4
NHEJ pathway
8oxo-dG*
APE1
LIG3
XRCC1
BER pathway
x3 replicates per age group
B
nissl+, NeuN+, Gad67- = PN class
nissl+, NeuN+, Gad67+ = IN class
cell class detection
subcellular compartment segmentation
nuclear POLK speckle detection
measure POLK & marker intensities within POLK speckles
C1
middle
early old
late old
gH2AX
POLK
gH2AX in speckels
POLK speckles
IN
PN
C2
R=0.49,p<2.2e-16
R=0.56,p<2.2e-16
R=0.092, p=0.019
R=0.43,p<2.2e-16
R=0.54,p<2.2e-16
R=0.065,p=0.048
Intensity gH2AX (A.U.)
Intensity Polk (A.U.)
C3
gH2AX
p=1.5 e-12, Cohen's d=0.32
p=7.5 e-06, Cohen's d=0.23
p=8.5 e-07, Cohen's d=0.2
error bar = 95% CLI
Nuclear Speckle Integrated Intensity (A.U.)
D1
53BP1
53BP1 in speckles
D2
R=0.49,p<2.2e-16
R=0.4,p<2.2e-16
R=0.4,p<2.2e-16
R=0.54,p<2.2e-16
R=0.4,p<2.2e-16
R=0.32,p<2.2e-16
Intensity 53BP1 (A.U.)
D3
53BP1
p<2 e-16 Cohen's d=0.83
p<2 e-16 Cohen's d=0.92
p=2.8 e-13 Cohen's d=0.46
E1
8oxo-dG
8oxo-dG in speckles
E2
R=0.31,p<2.2e-16
R=0.42,p<2.2e-16
R=0.55,p=2.7e-10
R=0.41,p<2.2e-16
R=0.51,p<2.2e-16
R=0.61,p=3.7e-15
Intensity 8oxo (A.U.)
E3
8oxo-dG
n.s.
p<2 e-16 Cohen's d=0.29
p=2.1 e-05 Cohen's d=0.28
F1
PRKDC
R=0.74 p<2.2e-16
R=0.54 p<2.2e-16
marker intensity (A.U.)
F2
APE1
R=0.4 p<2.2e-16
R=-0.048 p=0.15
F3
LIG3
R=0.25,p=6.7e-12
R=0.18 p=4.7e-06

Figure 3

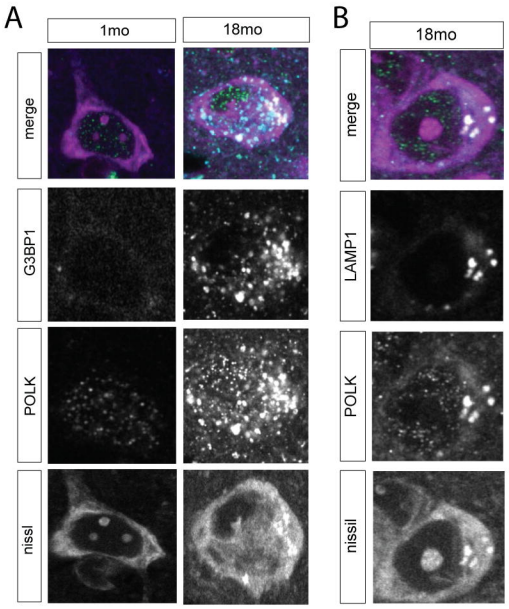

Figure 3

Figure 4

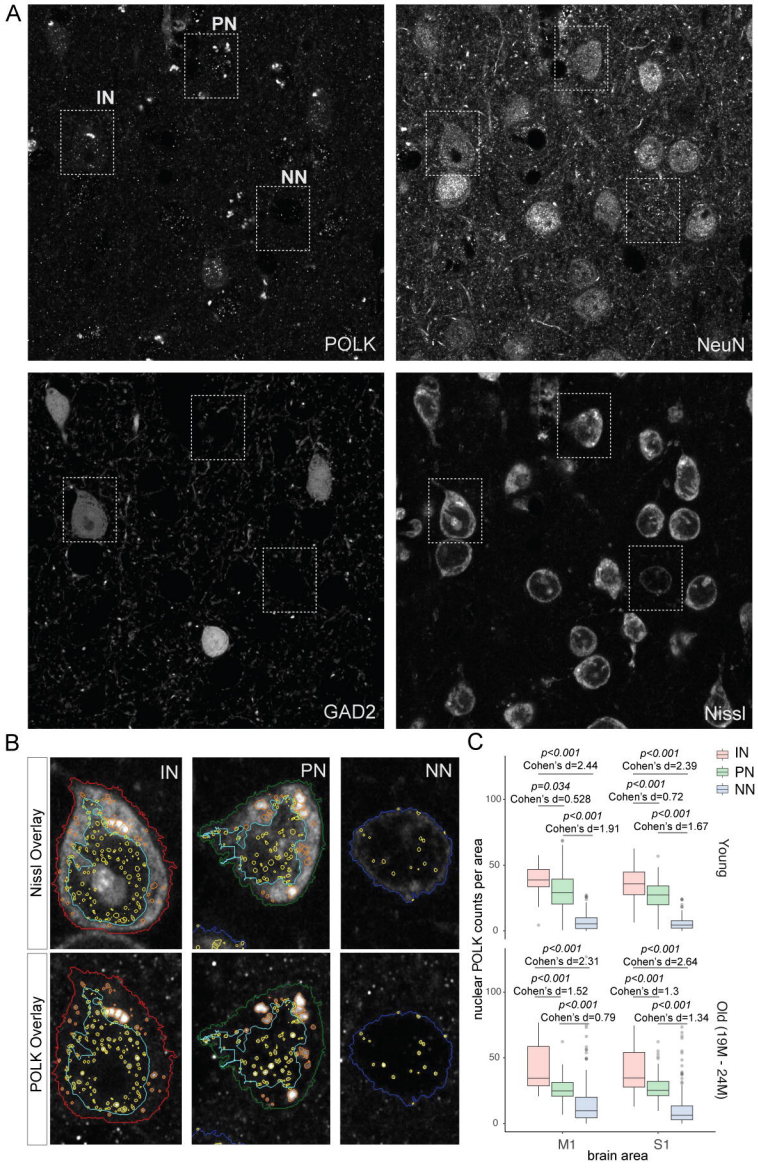
A
PN
IN
NN
POLK
NeuN
GAD2
Nissl
B
Nissl Overlay
POLK Overlay
IN
PN
NN
C
IN
PN
NN
p<0.001
Cohen's d=2.44
p<0.001
Cohen's d=2.39
p=0.034
Cohen's d=0.528
p<0.001
Cohen's d=0.72
p<0.001
Cohen's d=1.91
p<0.001
Cohen's d=1.67
Young
p<0.001
Cohen's d=2.31
p<0.001
Cohen's d=2.64
p<0.001
Cohen's d=1.52
p<0.001
Cohen's d=1.3
p<0.001
Cohen's d=0.79
p<0.001
Cohen's d=1.34
Old (19M - 24M)
nuclear POLK counts per area
100
50
0
M1
S1
brain area

Figure 5

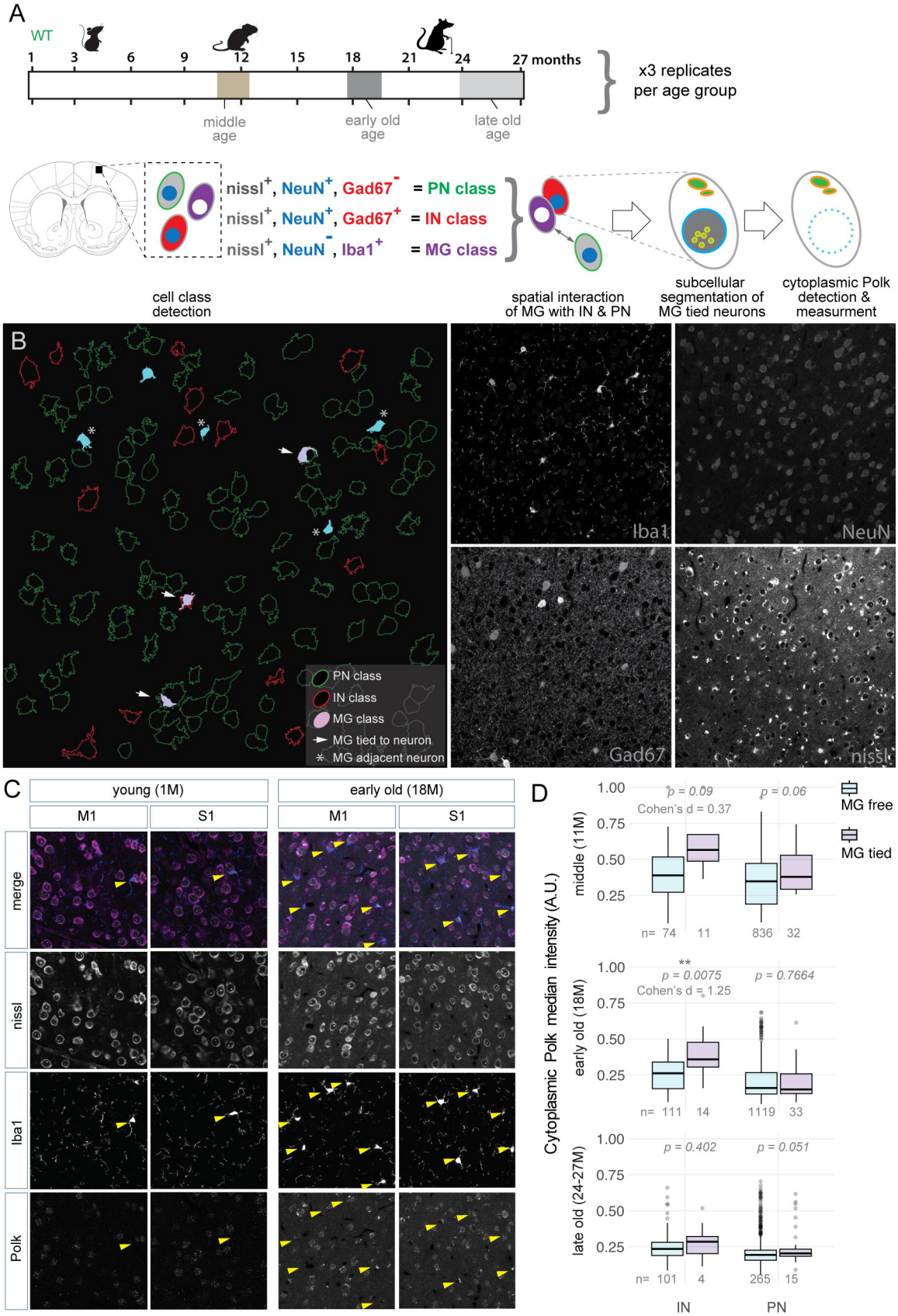
A
WT
1
3
6
9
12
15
18
21
24
27 months
x3 replicates per age group
middle age
early old age
late old age
nissl+, NeuN+, Gad67- = PN class
nissl+, NeuN+, Gad67+ = IN class
nissl+, NeuN-, Iba1+ = MG class
cell class detection
spatial interaction of MG with IN & PN
subcellular segmentation of MG tied neurons
cytoplasmic Polk detection & measurment
B
PN class
IN class
MG class
MG tied to neuron
MG adjacent neuron
Iba1
NeuN
Gad67
nissl
C
young (1M)
early old (18M)
M1
S1
merge
nissl
Iba1
Polk
D
Cytoplasmic Polk median intensity (A.U.)
middle (11M)
early old (18M)
late old (24-27M)
p = 0.09
Cohen's d = 0.37
p = 0.06
n= 74
11
836
32
**
p = 0.0075
Cohen's d = 1.25
p = 0.7664
n= 111
14
1119
33
p = 0.402
p = 0.051
n= 101
4
265
15
IN
PN
MG free
MG tied

Figure 6

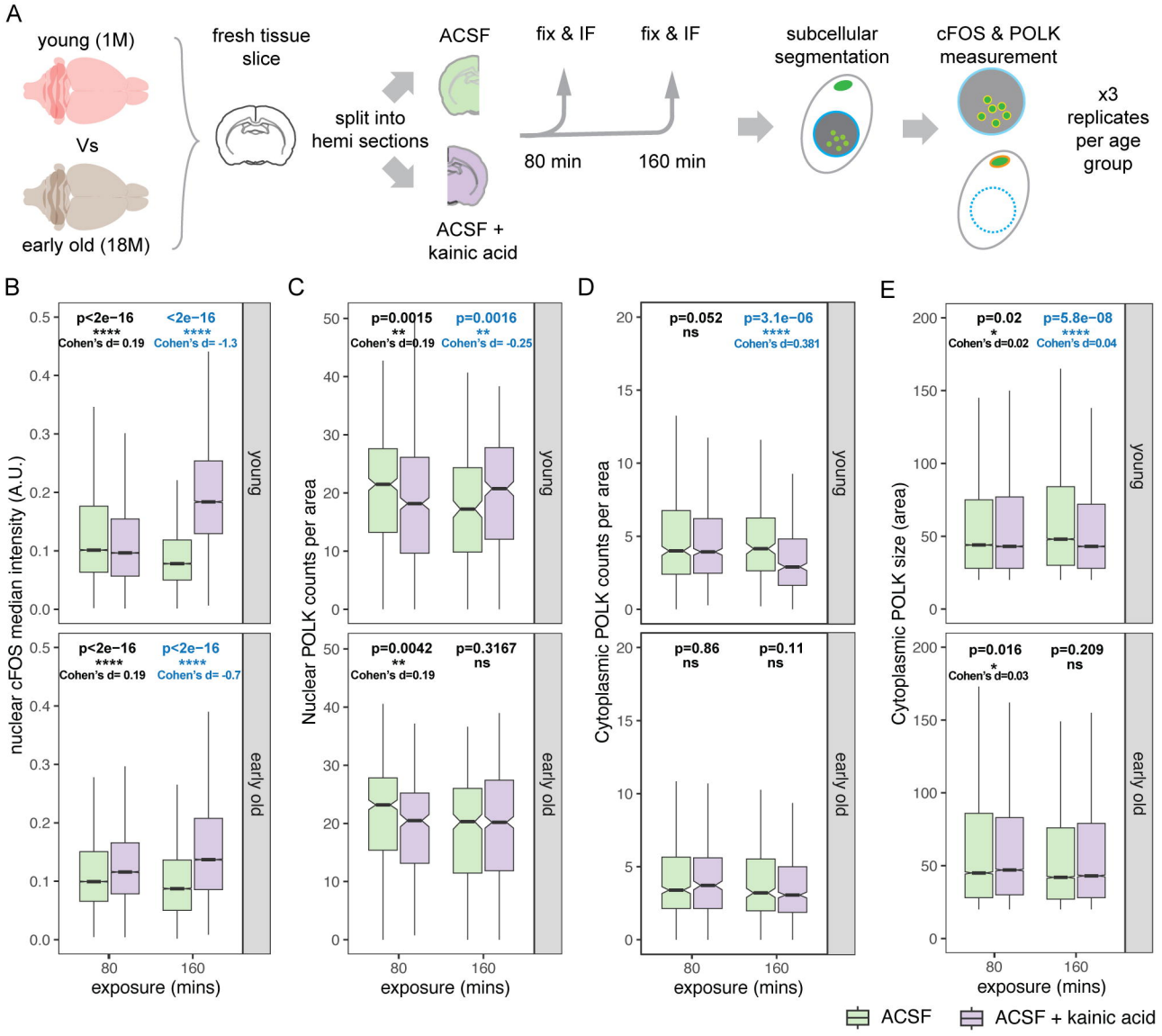
A
young (1M)
Vs
early old (18M)
fresh tissue slice
split into hemi sections
ACSF
ACSF + kainic acid
fix & IF
fix & IF
80 min
160 min
subcellular segmentation
cFOS & POLK measurement
x3 replicates per age group
B
nuclear cFOS median intensity (A.U.)
p<2e−16 **** Cohen's d= 0.19
<2e−16 **** Cohen's d= -1.3
p<2e−16 **** Cohen's d= 0.19
p<2e−16 **** Cohen's d= -0.7
young
early old
exposure (mins)
C
Nuclear POLK counts per area
p=0.0015 ** Cohen's d=0.19
p=0.0016 ** Cohen's d= -0.25
p=0.0042 ** Cohen's d=0.19
p=0.3167 ns
young
early old
exposure (mins)
D
Cytoplasmic POLK counts per area
p=0.052 ns
p=3.1e−06 **** Cohen's d=0.381
p=0.86 ns
p=0.11 ns
young
early old
exposure (mins)
E
Cytoplasmic POLK size (area)
p=0.02 * Cohen's d=0.02
p=5.8e−08 **** Cohen's d=0.04
p=0.016 * Cohen's d=0.03
p=0.209 ns
young
early old
exposure (mins)
ACSF
ACSF + kainic acid

Figure 7

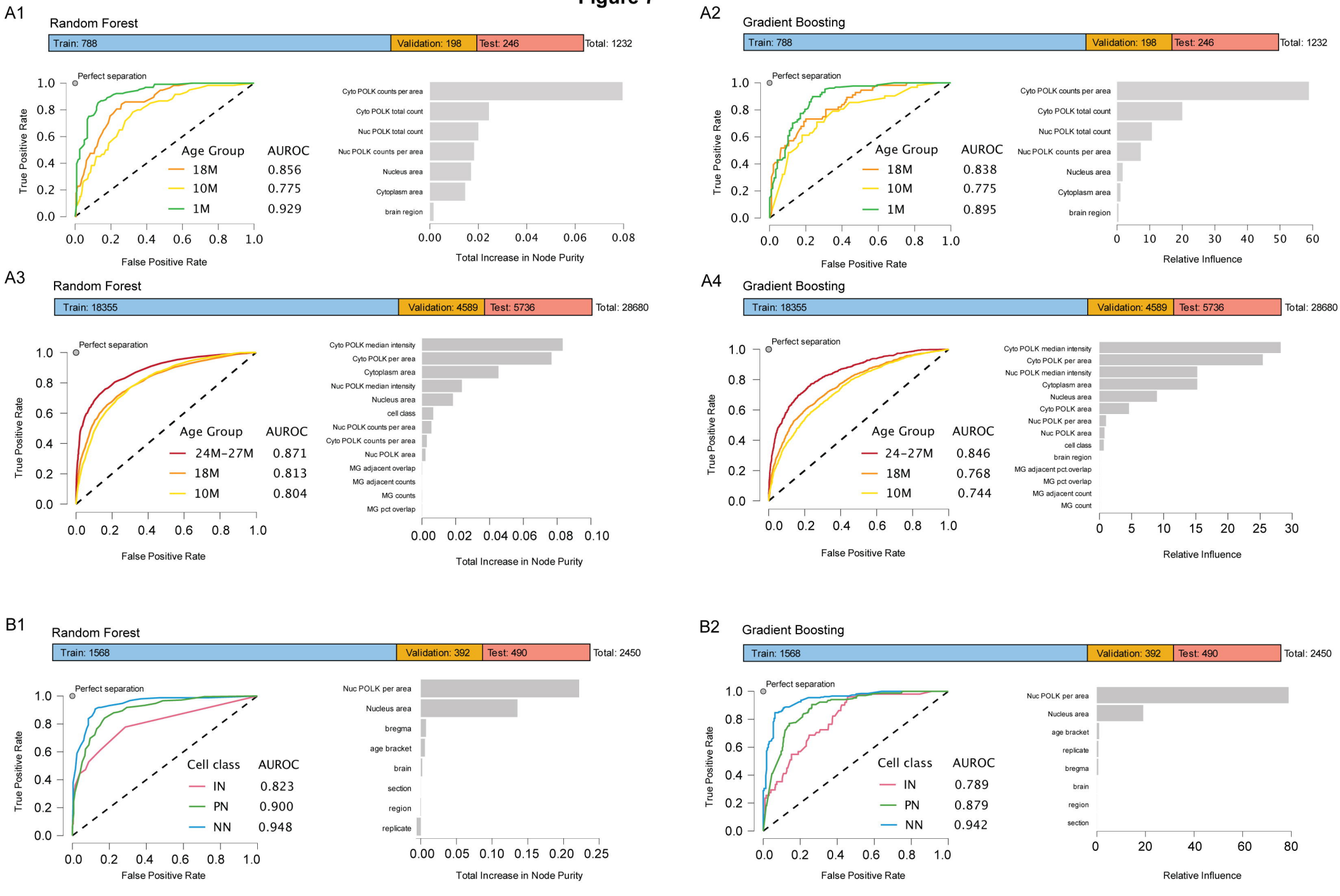
A1
Random Forest
Train: 788
Validation: 198
Test: 246
Total: 1232
Perfect separation
True Positive Rate
False Positive Rate
Age Group
AUROC
18M 0.856
10M 0.775
1M 0.929
Cyto POLK counts per area
Cyto POLK total count
Nuc POLK total count
Nuc POLK counts per area
Nucleus area
Cytoplasm area
brain region
Total Increase in Node Purity
A2
Gradient Boosting
Train: 788
Validation: 198
Test: 246
Total: 1232
Perfect separation
True Positive Rate
False Positive Rate
Age Group
AUROC
18M 0.838
10M 0.775
1M 0.895
Cyto POLK counts per area
Cyto POLK total count
Nuc POLK total count
Nuc POLK counts per area
Nucleus area
Cytoplasm area
brain region
Relative Influence
A3
Random Forest
Train: 18355
Validation: 4589
Test: 5736
Total: 28680
Perfect separation
True Positive Rate
False Positive Rate
Age Group
AUROC
24M-27M 0.871
18M 0.813
10M 0.804
Cyto POLK median intensity
Cyto POLK per area
Cytoplasm area
Nuc POLK median intensity
Nucleus area
cell class
Nuc POLK counts per area
Cyto POLK counts per area
Nuc POLK area
MG adjacent overlap
MG adjacent counts
MG counts
MG pct overlap
Total Increase in Node Purity
A4
Gradient Boosting
Train: 18355
Validation: 4589
Test: 5736
Total: 28680
Perfect separation
True Positive Rate
False Positive Rate
Age Group
AUROC
24-27M 0.846
18M 0.768
10M 0.744
Cyto POLK median intensity
Cyto POLK per area
Nuc POLK median intensity
Cytoplasm area
Nucleus area
Cyto POLK area
Nuc POLK per area
Nuc POLK area
cell class
brain region
MG adjacent pct.overlap
MG pct overlap
MG adjacent count
MG count
Relative Influence
B1
Random Forest
Train: 1568
Validation: 392
Test: 490
Total: 2450
Perfect separation
True Positive Rate
False Positive Rate
Cell class
AUROC
IN 0.823
PN 0.900
NN 0.948
Nuc POLK per area
Nucleus area
bregma
age bracket
brain
section
region
replicate
Total Increase in Node Purity
B2
Gradient Boosting
Train: 1568
Validation: 392
Test: 490
Total: 2450
Perfect separation
True Positive Rate
False Positive Rate
Cell class
AUROC
IN 0.789
PN 0.879
NN 0.942
Nuc POLK per area
Nucleus area
age bracket
replicate
bregma
brain
region
section
Relative Influence

Absolute counts of nuclear Polk speckles

Table 1.1

ANCOVA Post Hoc Comparisons - age, with nuclear area as covariate

		Mean Diff	SE	t	Cohen's d	p_{tukey}		p_{bonf}	
1M	10M	18.432	1.806	10.203	0.854	< .001	***	< .001	***
1M	18M	20.584	1.918	10.733	0.954	< .001	***	< .001	***
10M	18M	2.152	2.212	0.973	0.1	0.594		0.992	

Note. Results are averaged over the levels of: brain area
Note. P-value adjusted for comparing a family of 3
* p < .05, ** p < .01, *** p < .001

Table 1.2

ANCOVA Post Hoc Comparisons - age ∗ brain area, with nuclear area as covariate

		Mean Diff	SE	t	Cohen's d	p_{tukey}		p_{bonf}	
1M Cg1	10M Cg1	22.276	4.841	4.602	1.032	< .001	***	< .001	***
1M Cg1	18M Cg1	25.265	4.987	5.066	1.171	< .001	***	< .001	***
10M Cg1	18M Cg1	2.99	5.881	0.508	0.139	1		1	
1M M1	10M M1	18.729	3.366	5.564	0.868	< .001	***	< .001	***
1M M1	18M M1	24.795	3.341	7.421	1.149	< .001	***	< .001	***
10M M1	18M M1	6.066	3.976	1.526	0.281	0.933		1	
1M M2	10M M2	17.852	3.576	4.992	0.827	< .001	***	< .001	***
1M M2	18M M2	14.258	4.105	3.474	0.661	0.026	*	0.035	*
10M M2	18M M2	-3.593	4.699	-0.765	-0.167	1		1	
1M S1	10M S1	14.873	2.117	7.027	0.689	< .001	***	< .001	***
1M S1	18M S1	18.018	2.057	8.758	0.835	< .001	***	< .001	***
10M S1	18M S1	3.144	2.293	1.371	0.146	0.969		1	

Note. P-value adjusted for comparing a family of 12, only relevant comparisons are shown
* p < .05, ** p < .01, *** p < .001

Size (area) of nuclear Polk speckles

Table 2.1

ANOVA Post Hoc Comparisons - age

		Mean Differen	SE	t	Cohen's d	p_{tukey}		p_{bonf}	
1M	10M	7.195	0.431	16.708	0.099	< .001	***	< .001	***
1M	18M	23.617	0.578	40.861	0.323	< .001	***	< .001	***
10M	18M	16.422	0.653	25.143	0.225	< .001	***	< .001	***

Note. Results are averaged over the levels of: brain area
Note. P-value adjusted for comparing a family of 3
* p < .05, ** p < .01, *** p < .001

Table 2.2

ANOVA Post Hoc Comparisons - age ∗ area

		Mean Diff	SE	t	Cohen's d	p_{tukey}		p_{bonf}	
1M Cg1	10M Cg1	12.882	1.11	11.6	0.176	< .001	***	< .001	***
1M Cg1	18M Cg1	25.397	1.534	16.56	0.348	< .001	***	< .001	***
10M Cg1	18M Cg1	12.516	1.714	7.304	0.171	< .001	***	< .001	***
1M M1	10M M1	3.105	0.877	3.542	0.043	0.02	*	0.026	*
1M M1	18M M1	23.945	1.035	23.125	0.328	< .001	***	< .001	***
10M M1	18M M1	20.841	1.248	16.697	0.285	< .001	***	< .001	***
1M M2	10M M2	10.629	0.805	13.196	0.146	< .001	***	< .001	***
1M M2	18M M2	24.644	1.263	19.512	0.338	< .001	***	< .001	***
10M M2	18M M2	14.015	1.365	10.27	0.192	< .001	***	< .001	***
1M S1	10M S1	2.165	0.563	3.847	0.03	0.007	**	0.008	**
1M S1	18M S1	20.483	0.571	35.892	0.281	< .001	***	< .001	***
10M S1	18M S1	18.318	0.685	26.749	0.251	< .001	***	< .001	***

Note. P-value adjusted for comparing a family of 12, only relevant comparisons are shown
* p < .05, ** p < .01, *** p < .001

Absolute counts of cytoplasmic Polk granules

Table 3.1

Post Hoc Comparisons - age, with cytoplasmic area as covariate

		Mean Diff	SE	t	Cohen's d	p_{tukey}		p_{bonf}	
1M	10M	18.432	1.806	10.203	0.854	< .001	***	< .001	***
1M	18M	20.584	1.918	10.733	0.954	< .001	***	< .001	***
10M	18M	2.152	2.212	0.973	0.1	0.594		0.992	

Note. Results are averaged over the levels of: brain area
Note. P-value adjusted for comparing a family of 3
* p < .05, ** p < .01, *** p < .001

Table 3.2

ANCOVA Post Hoc Comparisons - age ∗ brain area, with cytoplasmic area as covariate

		Mean Diff	SE	t	Cohen's d	p_{tukey}		p_{bonf}	
1M Cg1	10M Cg1	57.944	10.232	5.663	1.27	< .001	***	< .001	***
1M Cg1	18M Cg1	80.174	10.502	7.634	1.757	< .001	***	< .001	***
10M Cg1	18M Cg1	22.23	12.432	1.788	0.487	0.824		1	
1M M1	10M M1	59.109	7.094	8.333	1.295	< .001	***	< .001	***
1M M1	18M M1	60.769	7.009	8.67	1.332	< .001	***	< .001	***
10M M1	18M M1	1.661	8.403	0.198	0.036	1		1	
1M M2	10M M2	58.471	7.572	7.722	1.281	< .001	***	< .001	***
1M M2	18M M2	66.588	8.679	7.672	1.459	< .001	***	< .001	***
10M M2	18M M2	8.117	9.896	0.82	0.178	1		1	
1M S1	10M S1	60.836	4.466	13.623	1.333	< .001	***	< .001	***
1M S1	18M S1	57.122	4.343	13.153	1.252	< .001	***	< .001	***
10M S1	18M S1	-3.713	4.853	-0.765	-0.081	1		1	

Note. P-value adjusted for comparing a family of 12, only relevant comparisons are shown
* p < .05, ** p < .01, *** p < .001

Size (area) of cytoplasmic Polk granules

Table 4.1

Post Hoc Comparisons - age

		Mean Diff	SE	t	Cohen's d	p_{tukey}		p_{bonf}	
1M	10M	-12.531	0.667	-18.778	-0.066	< .001	***	< .001	***
1M	18M	-47.599	0.904	-52.653	-0.252	< .001	***	< .001	***
10M	18M	-35.068	1.036	-33.834	-0.186	< .001	***	< .001	***

Note. Results are averaged over the levels of: area
Note. P-value adjusted for comparing a family of 3
*** p < .001

Table 4.2

Post Hoc Comparisons - age ∗ area

		Mean Diff	SE	t	Cohen's d	p_{tukey}		p_{bonf}	
1M Cg1	10M Cg1	-13.423	1.666	-8.057	-0.071	< .001	***	< .001	***
1M Cg1	18M Cg1	-51.086	2.545	-20.074	-0.27	< .001	***	< .001	***
10M Cg1	18M Cg1	-37.662	2.845	-13.236	-0.199	< .001	***	< .001	***
1M M1	10M M1	-16.06	1.382	-11.619	-0.085	< .001	***	< .001	***
1M M1	18M M1	-58.375	1.472	-39.662	-0.309	< .001	***	< .001	***
10M M1	18M M1	-42.314	1.853	-22.832	-0.224	< .001	***	< .001	***
1M M2	10M M2	-4.69	1.308	-3.585	-0.025	0.018	*	0.022	*
1M M2	18M M2	-46.978	1.951	-24.076	-0.249	< .001	***	< .001	***
10M M2	18M M2	-42.288	2.164	-19.544	-0.224	< .001	***	< .001	***
1M S1	10M S1	-15.95	0.853	-18.698	-0.084	< .001	***	< .001	***
1M S1	18M S1	-33.958	0.791	-42.926	-0.18	< .001	***	< .001	***
10M S1	18M S1	-18.008	0.988	-18.231	-0.095	< .001	***	< .001	***

Note. P-value adjusted for comparing a family of 12, only relevant comparisons are shown
* p < .05, ** p < .01, *** p < .001

Table 5.1

Cell class nuclear Polk counts per area

Post Hoc Comparisons - age_bracket ∗ Cell-type

		Mean Diff	SE	t	Cohen's d	p_{tukey}	
young IN	young PN	7.593	1.276	5.948	0.624	< .001	***
young IN	young NN	29.403	1.266	23.231	2.418	< .001	***
young PN	young NN	21.81	0.721	30.252	1.793	< .001	***
early old IN	early old PN	17.191	1.391	12.362	1.414	< .001	***
early old IN	early old NN	30.189	1.352	22.333	2.482	< .001	***
early old PN	early old NN	12.998	0.762	17.066	1.069	< .001	***

Note. Results are averaged over the levels of: area

Note. P-value adjusted for comparing a family of 6, only relevant comparisons shown

*** p < .001

Table 5.2

Post Hoc Comparisons - age_bracket ∗ Cell-type ∗ area

		Mean Diff	SE	t	Cohen's d	p_{tukey}	
young IN M1	young PN M1	6.422	1.891	3.396	0.528	0.034	*
young IN M1	young NN M1	29.677	1.872	15.854	2.44	< .001	***
young PN M1	young NN M1	23.255	1.079	21.549	1.912	< .001	***
young IN S1	young PN S1	8.764	1.715	5.111	0.721	< .001	***
young IN S1	young NN S1	29.129	1.704	17.094	2.395	< .001	***
young PN S1	young NN S1	20.366	0.956	21.297	1.675	< .001	***
early old IN M1	early old PN M1	18.541	1.997	9.282	1.525	< .001	***
early old IN M1	early old NN M1	28.156	1.945	14.474	2.315	< .001	***
early old PN M1	early old NN M1	9.615	1.159	8.296	0.791	< .001	***
early old IN S1	early old PN S1	15.842	1.935	8.185	1.303	< .001	***
early old IN S1	early old NN S1	32.222	1.878	17.162	2.649	< .001	***
early old PN S1	early old NN S1	16.38	0.988	16.571	1.347	< .001	***

Note. P-value adjusted for comparing a family of 12, only relevant comparisons shown

* p < .05, ** p < .01, *** p < .001